Assessment of the landslide dams in Western Austria, Bavaria and Northern Italy (part of the Eastern Alps): Data inventory development and application of geomorphic indices

Roshanak Shafieiganjeh [a,*], Marc Ostermann [b], Barbara Schneider-Muntau [c], Bernhard Gems [a]

[a] *Unit of Hydraulic Engineering, University of Innsbruck, Technikerstraße 13, 6020 Innsbruck, Austria*
[b] *Geological Survey of Austria, Neulinggasse 38, 1030 Vienna, Austria*
[c] *Unit of Geotechnical and Tunnel Engineering, University of Innsbruck, Technikerstraße 13, 6020 Innsbruck, Austria*

ABSTRACT

Landslide dams pose significant hazards towards their upstream and downstream areas due to damming and flooding. Case studies and the use of geomorphic indices, which are developed based on large datasets, are two common approaches in the stability assessment of landslide dams. To gain an insight into the evolution of landslide dams within a part of the Eastern Alps and to provide a basis for further studies on this topic, a data inventory including 73 landslide dams is presented. The database covers sites in Western Austria, Bavaria and Northern Italy, containing 39 descriptive and quantitative parameters gathered in five categories of location, landslide, dam, lake, and catchment. The methodologies utilized for parameter definition follow a simple and consistent procedure described in detail for one case study, the Wiese landslide in Tyrol (Austria). Statistical assessment of the geometric parameters indicated an acceptable collation between mean values of the developed inventory and dataset of other geographical regions. Moreover, by developing a correlation matrix of the quantitative fields, landslide dam parameters showed a fairly strong correlation with the landslide and backwater lake parameters. However, they appear to be statistically independent of the catchment area characteristics. The applicability of the previously developed geomorphic indices is evaluated by plotting the current data and determining the upper and lower bounds of the stable and unstable domains regarding a 95 % confidence level of the mean value. The best applicability is obtained out of the blockage and dimensionless blockage indices. Further, a set of catchment ruggedness-based indices are developed based on the collected data. The indices act upon the catchment properties as driving forces and three different sets of characteristics of the dam and landslide as resisting forces. The reliability of these indices is confirmed by obtaining the adjusted R^2 within 70–85 %, narrowing down the uncertain domain on the graphs in comparison to the reviewed literature, and the applicability of them on the current database. Each catchment ruggedness-based index is suitable to predict the evolution of the dams and backwater lakes at the time of occurrence depending on the available data.

1. Introduction

Landslide dams are naturally-formed obstructions of water courses caused by slope failures. They are mostly formed where narrow steep valleys are bordered by high rugged mountains (Costa and Schuster, 1988). The backwater lakes that form as the result of river blockage can pose significant hydraulic off-site risks upstream due to damming effects and downstream due to flooding. As an example, the failure of a 16 Mm³ landslide on the Savio river in Quarto, Italy in 1812, caused 18 casualties

due to drowning (Bertoni, 1843). According to Costa and Schuster (1988), half of the landslide dams only last 10 days after their formation. However, landslide dams have shown a various range of longevity from several minutes to centuries based on the factors such as volume, size, shape, sorting of blockage material, rate of seepage through the material, and rate of water and sediment inflow (Costa and Schuster, 1988; Peng and Zhang, 2012). The deadliest natural dam failure occurred 10 days after the formation of a huge landslide dam on Daru River (China, 1786), where the flood due to dam breach extended 1400 km

---

Fig. 1. Location of the landslide dams involved in the database. The cases located in Austria, Italy and Germany are shown on the 10 m resolution terrain model from Airborne Laser scan data in the projection EPSG: 31287 (www.geoland.at).

downstream and drowned 100,000 people (Dai et al., 2005). On the other hand, Kummer lake (Kummersee) in South Tyrol, Italy, went through a catastrophic outburst 370 years after its formation causing fatalities and destruction of Merano village (Eisbacher and Clague, 1984; Pirocchi, 1992). Given the broad and unknown failure time of the landslide dams, and the placement of many infrastructures and settlements at the valley floors (Casagli and Ermini, 1999), the evaluation of the landslide dams' stability is important to prevent further damages and destructions.

Detailed field studies along with measurements on single cases and inventories are accounted as the foremost sources in the apprehension of stability, failure, and consequences of landslide dams (Korup and Wang, 2015). Many single studies on huge landslide dams have been presented in the literature (Schuster and Alford, 2004; Dai et al., 2005; Ostermann et al., 2012; Delaney and Evans, 2015; Wang et al., 2016). Moreover, several landslide dam inventories have been developed for different parts of the world including Italy with 70 cases (Casagli and Ermini, 1999) and 300 cases (Tacconi Stefanelli et al., 2015), Venezuela with 35 cases (Ferrer, 1999), a worldwide database consisting of 350 cases (Ermini and Casagli, 2003), New Zealand with 232 cases (Korup, 2004) and 240 cases (Korup, 2011), Japan with 43 cases (Dong et al., 2009), Switzerland with 35 cases (Bonnard, 2011), Central Andes of Argentina with 20 cases in Argentine Northwest and 41 cases in Northern Patagonia (Hermanns et al., 2011a), Karakoram Himalaya with 322 cases (Hewitt, 2011), China with 828 cases (Fan et al., 2012), Central Asia with 190 cases (Strom and Abdrakhmatov, 2018), and Peru with 51 cases (Tacconi Stefanelli et al., 2018).

Landslides are a relatively common phenomenon in the Alpine region to the extent that, the Quaternary valley evolution in the Tyrolean Alps (Austria) is mostly specified as the result of several deep-seated mass movements (Prager et al., 2008). The first inventory on the Alpine region landslides also including landslide dams has been developed by Abele (1974), in which 79 landslides (catastrophic rockslides or

rock avalanches) have been listed from the Eastern Alps area while some geometrical characteristics such as landslide runout length, runout angle, area, and volume have been estimated. Costa and Schuster (1991) archived 13 Austrian landslide dams in a worldwide inventory of historical landslide dams however, the presented information mostly included the locality of the dams and the type of the landslide. In the past twenty years, many studies have been conducted and characterized the landslide dams in Western Austria, Northern Italy, and Bavaria (Felber, 1987; Poschinger and Thom, 1995; Ivy-Ochs et al., 1998; Jerz, 1999; Schrott et al., 2003; Uhlir and Schramm, 2003; Morche et al., 2006; Prager et al., 2006; Reuther et al., 2006; Ostermann et al., 2007; Prager et al., 2008; Cotza, 2009; Gruber et al., 2009; Prager et al., 2009a; Prager et al., 2009b; Panizza et al., 2011; Ostermann et al., 2012; Patzelt, 2012; Starnberger et al., 2013; Stefani et al., 2013; Dufresne et al., 2016; Ostermann and Prager, 2016; Ostermann and Sanders, 2017; Ostermann et al., 2017; Dufresne et al., 2018; Knapp et al., 2020; Ostermann et al., 2020; Reitner et al., 2020; Zangerl et al., 2020). Although, a comprehensive database that encompasses detailed information on the geomorphological and geometrical characteristics of these landslide dams is lacking in the literature.

The common practice for landslide dams' inventories is to assess the variation of single geometric parameters for a high number of stable and unstable cases. By employing the statistical analysis of these parameters, geomorphic indices have been developed (Ermini and Casagli, 2003; Korup, 2004; Tacconi Stefanelli et al., 2016; Dufresne et al., 2018). Landslide dam's stability can be predicted by geomorphic indices based on physical characteristics of the landslide and the dam as resisting strength, and the formed lake and the catchment area upstream of the point of blockage (the intersection of dammed river and landslide material) as a destructive force. The geomorphic indices are rather simple relationships as their main objective is to gain a general idea about the stability of formed dams or backwater lakes (Tacconi Stefanelli et al., 2016). Therefore, required parameters should be taken in a fast and easy

2
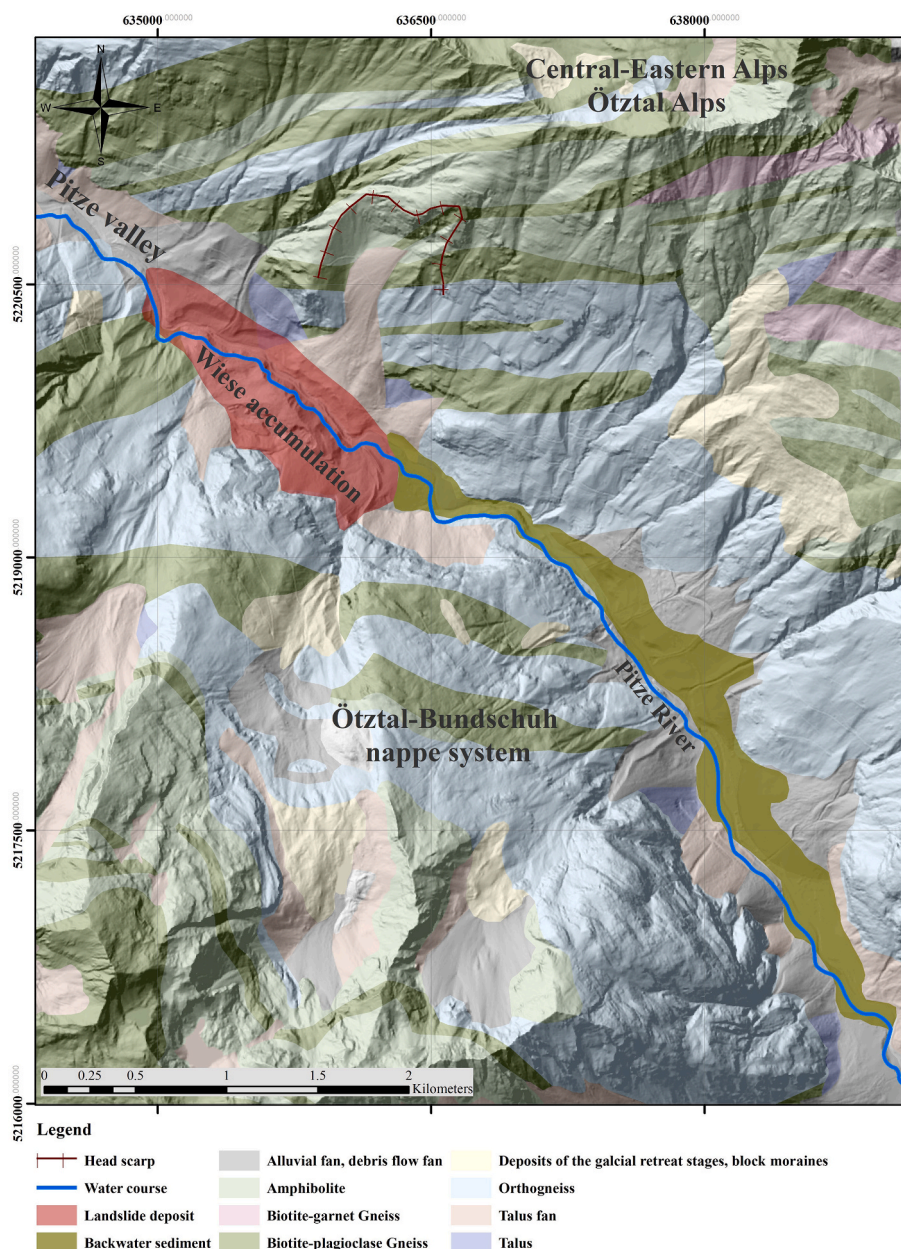
Fig. 2. The scarp and dam accumulation of the Wiese landslide and the backwater sediments due to damming of the Pitze river in the Pitze valley (Pitztal) are displayed on the geological units of the surrounding areas (1:50,000 geological map, gisgba.geologie.ac.at) and 5 m DEM of Tyrol, Austria (data.gv.at). According to the tectonic map of Schmid et al. (2004), the study area of the Wiese landslide completely lies within the Ötztal-Bundschuh nappe system.

data collection system, so that they could be utilized in emergencies.

This study aims to firstly develop a GIS-based inventory for landslide dams in Western Austria, Northern Italy, and Bavaria based on their physical and geometrical characteristics proposing relatively accurate and simple methods utilized in measuring these parameters. Consequently, the existence of a comprehensive database for this region provides the chance of examining the applicability of the previously developed geomorphic indices on the elaborated inventory and, at the same time, carrying out a comparison with results of other geographic regions. Depending on the trend of the measured parameters for stable and unstable landslide dams of the data inventory, a new set of geomorphic indices based on the watershed properties as a destructive force and three different resisting forces relating to the landslide and dam is proposed. They enhanced the prediction efficiency of the landslide dam's evolution in the Eastern Alps by narrowing down the uncertain domain and providing different possibilities for the stability

estimation regarding the available data in case of an emergency.

2. Data and methods

2.1. Data collection

The starting point to define the landslide dams of the inventory was the detailed analysis of the landslides classified in Abele (1974) in the Eastern Alps region. The process of discriminating landslide dams out of the listed landslides is carried out by analyzing the satellite images on Google Earth and 2.5–10 meter cell-size Digital Elevation Models (DEM) (data.gv.at, geokatalog.bürgernetz.bz.it, ldbv.bayern.de, geoland.at). Moreover, clusters of landslide dams in certain valleys (Prager et al., 2008; Ostermann and Prager, 2016; Ostermann and Sanders, 2017; Dufresne et al., 2018; Ostermann et al., 2020) and case-study-based researches (Poschinger and Thom, 1995; Uhlir and Schramm, 2003;
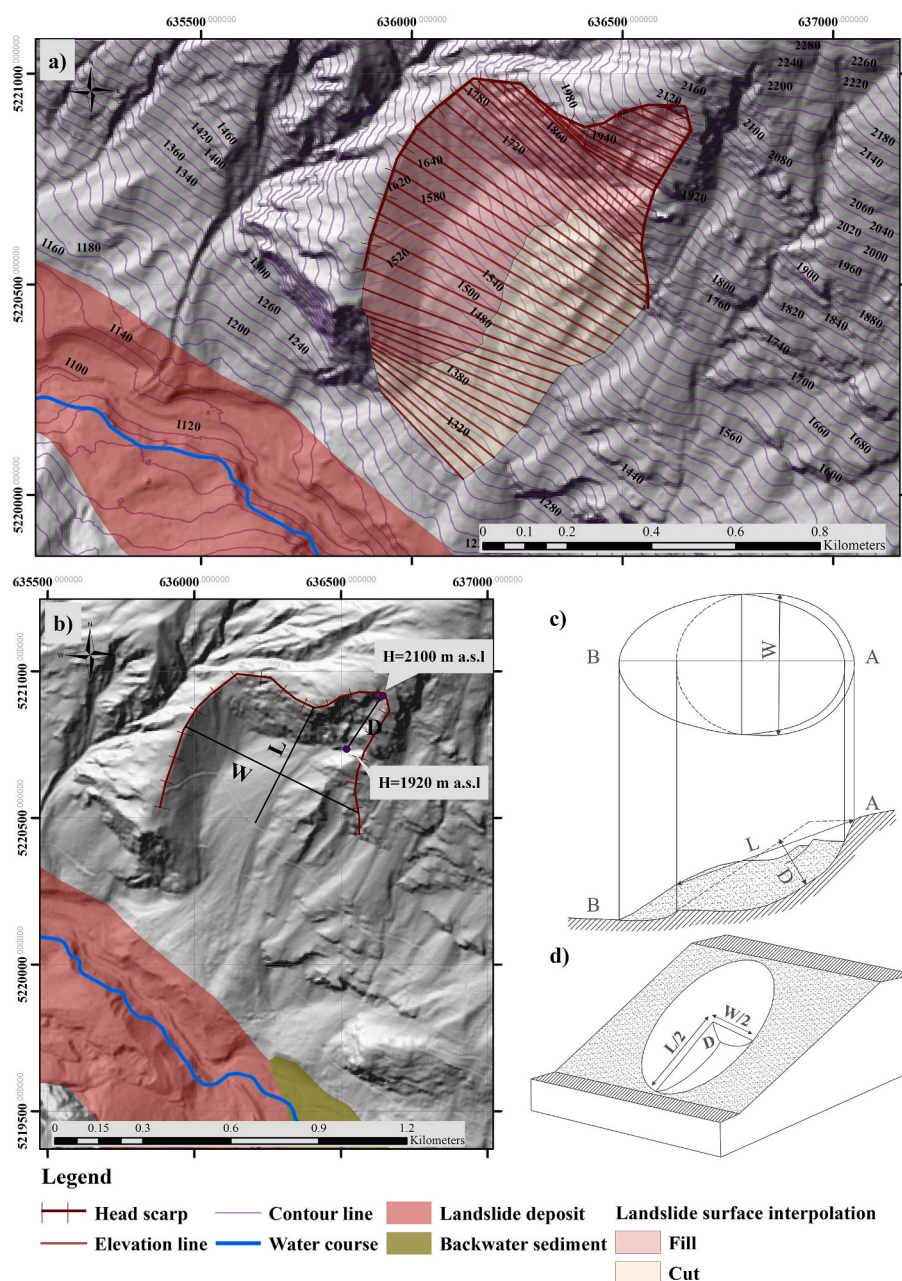
Fig. 3. The process of the landslide volume estimation is displayed for the Wiese landslide. (a) The resulted surface difference of the current topography and the planar surface created by the elevation lines is shown in two parts of cut and fill. The volume of the fill segment is assigned as the landslide volume. (b) The estimation of landslide volume according to the geometric parameters is presented. The width (W), length (L), and approximation of depth (D) of the surface of rupture are shown (5 m DEM of Tyrol, Austria (data.gv.at)) (c) The dimensions of the parameters required for the landslide volume calculation are shown on a schematic cross-section for a typical rotational landslide. (d) Portion of a schematic slope indicating the estimation of the landslide volume by assuming it as a half-ellipsoid shape (Curden and Varnes, 1996).

Morche et al., 2006; Prager et al., 2006; Gruber et al., 2009; Prager et al., 2009b; Ostermann et al., 2012; Patzelt, 2012; Dufresne et al., 2016; Ostermann et al., 2017; Knapp et al., 2020; Reitner et al., 2020; Zangerl et al., 2020) have been addressed widely in the literature. After a case-by-case geomorphic inspection, and determination of the scarp area of the landslides, dams' border, and backwater sediments or current lake extension, 73 landslide dams were listed in this inventory (Fig. 1).

The database mainly covers parameters that can be measured systematically and which are relevant for assessing the landslide dam stability. The data is gathered in five categories, covering location, landslide, dam, lake, and catchment (Table A.1). In the following sections, the methods used for the measurements of different quantitative parameters are described in detail through one example of the database. The landslide dam number 72, Wiese, is selected as no detailed previous survey or parameter calculation has been performed there.

2.2. Location

In this category the coordinate of the landslide's scarp and deposit centroid, the geographic position of the landslide dams within the political borders, their position in the Alps, the specific mountain group based on Graßler's (1984) classification, and the river either blocked or diverted by the landslide accumulation are stated.

As an example, the Wiese landslide with the scarp coordinate of 63,633.81 E, 5220941.71 N is located in the Tyrol province of Austria. The landslide lays in the Central-Eastern part of the Ötztal Alps in Pitz valley (Pitztal) and dammed the Pitze river (Fig. 2).

2.3. Landslide

In the landslide field, general and quantitative information about the landslide process is presented. The age of almost half of the landslides is stated based on radiometric dating studies in the literature. The mea-
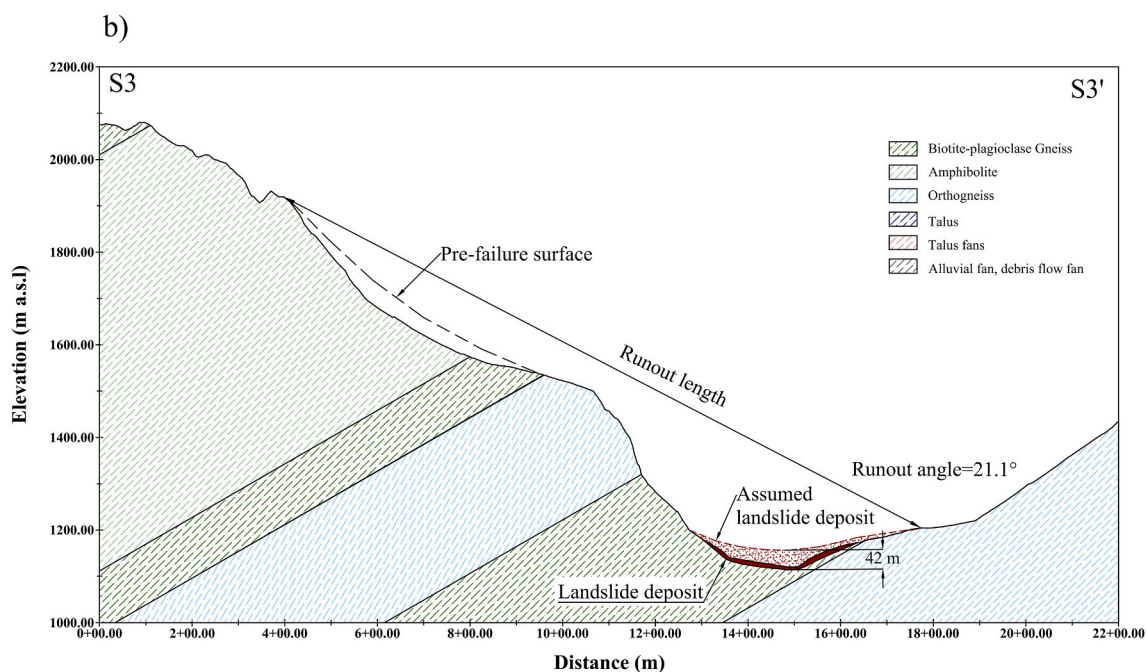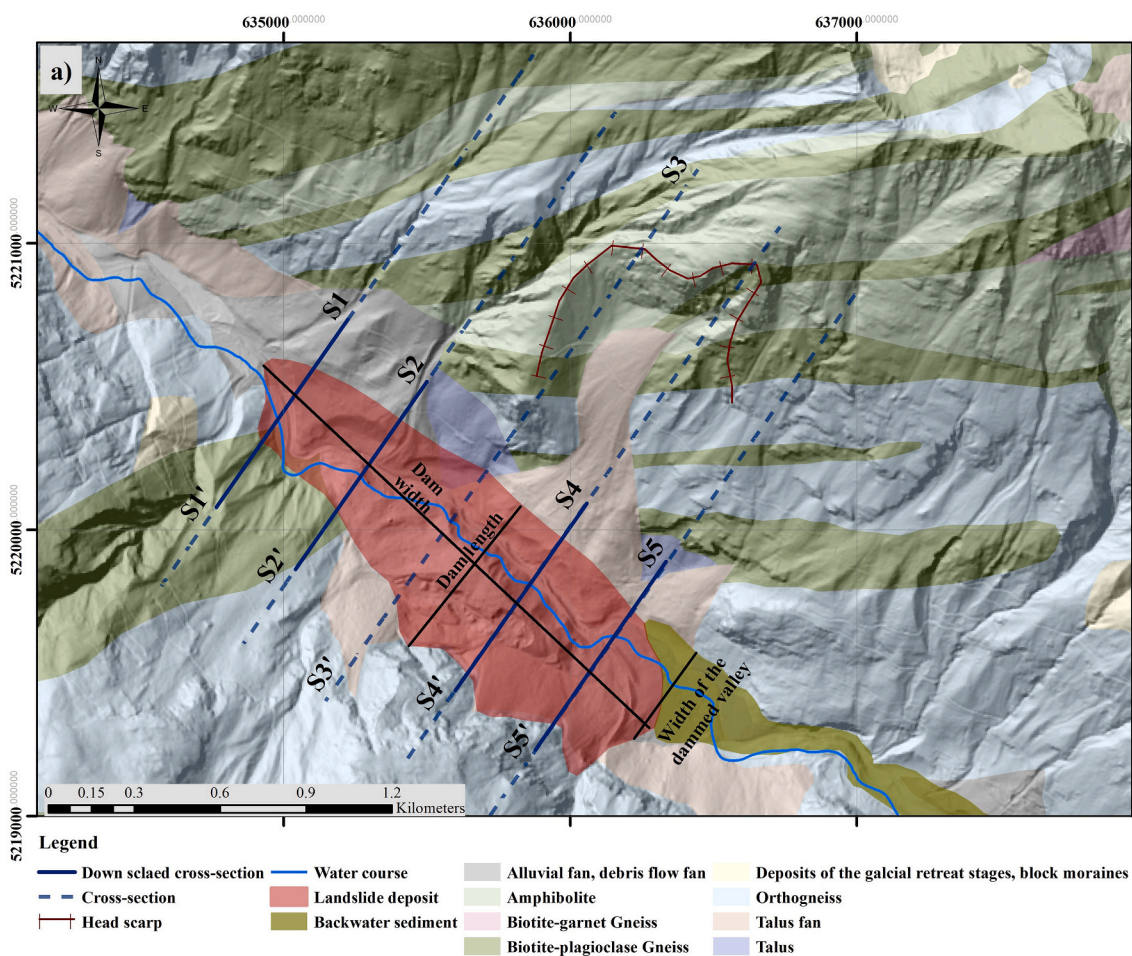
Fig. 4. Height estimation steps of Wiese dam accumulation are shown. a) The geometrical parameters of the dam and cross-sections are displayed on the 5 m DEM of Tyrol, Austria (data.gv.at) and the geological units (1:50,000 geological map, gisgba.geologie.ac.at). b) Landslide geometrical parameters are displayed on cross-section number 3. The shown pre-failure surface is almost equal to the sum of the assumed landslide deposit (the area under the dashed line) and the determined surface beneath the current valley floor (the solid part). c) The shape of the valley floor and the assumed landslide deposit for cross-sections 1, 2, 4, and 5 are shown in a down-scaled format.

c)
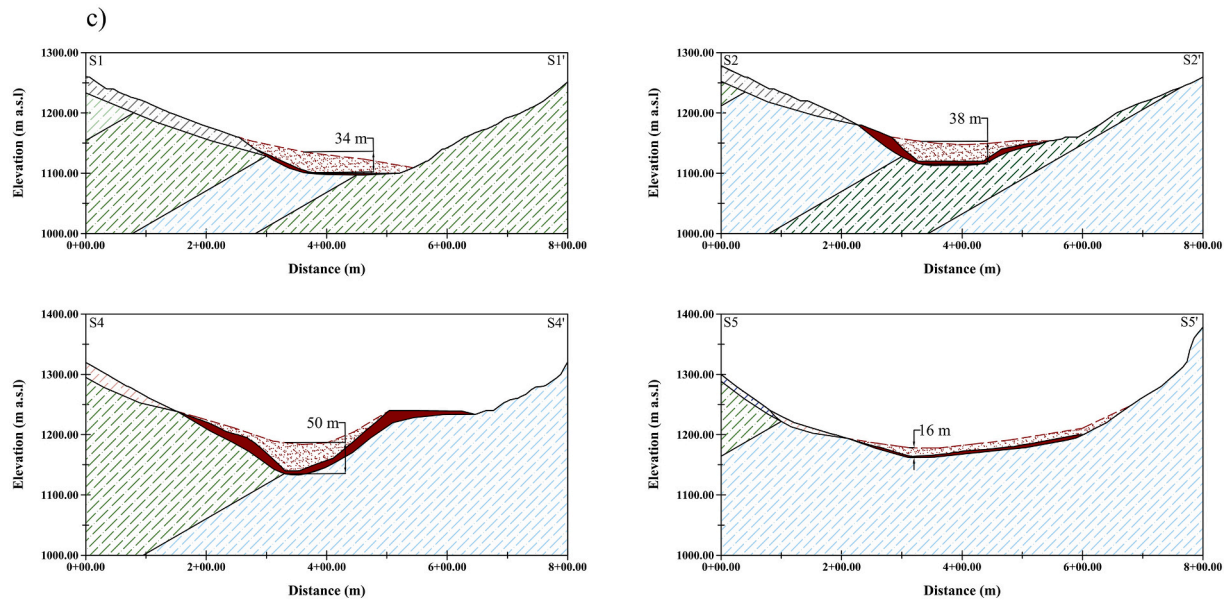
Fig. 4. (*continued*).

surement of the difference in height between crown and tip of each landslide (H_L) and the straight-line distance from crown to tip (R_L) allows the calculation of the runout angle (R_A) (Curden and Varnes, 1996). The estimation of the landslide volume is carried out first based on data previously stated in literature where available. For the rest of the cases, two methods are implemented: (1) the volume is approximated based on the prolongation and extrapolation of contour lines in 20 m intervals for the pre-landslide situation. The reconstruction of the landslides is carried out by creating a planar surface between contours with the same elevation at both sides of the landslide flanks (Ostermann and Prager, 2016; Dufresne et al., 2018; Reitner et al., 2020), (2) the landslide is considered as half-ellipsoid in which its volume can be calculated using the equation developed by Curden and Varnes (1996):

$$V = \frac{1}{6}\pi DWL \tag{1}$$

where D is the maximum depth of the surface of rupture below the original ground surface, W is the width of the surface of rupture which is the maximum distance between the flanks of the landslide perpendicular to the length, and L is the length of the surface of rupture that is the minimum distance from the toe of the surface of rupture to the crown (Fig. 3-b). To estimate the depth of the surface of rupture under the displaced materials, methods such as detailed site investigations (Hutchinson, 1983), developing statistical relations based on landslides inventories, and use of high-resolution DEMs (Bunn et al., 2020; Domej et al., 2020) have been proposed. Here, in the concept of creating a landslide dam database, a rough estimation of the depth of the surface of rupture based on the height of the exposed part of the main scarp is implemented. Though, due to the lower precision compared to the contour lines extrapolation, the obtained values of this method are only used to control the range of the prior.

The Wiese landslide which is comprised of Biotite-plagioclase Gneiss and Amphibolite in the upper part and Orthogneiss in the lower part lies in the Ötztal-Bundschuh nappe system (Fig. 2). According to 2100 m a.s. l. elevation at the scarp, the difference in height of the landslide is estimated to be about 800 m. The maximum horizontal distance between the crown and the tip is equal to 2 km consequently, the calculated runout angle is 21.1°. The volume of the landslide is estimated to be 12 Mm^3 by reconstructing the surface before the event (Fig. 3-a) and 14 Mm^3 considering 180 m depth of the surface of rupture (Fig. 3-b). The same relation between the results of the two methods also exists for most

of the other cases which shows a slight overestimation of the landslide volume in the second approach. This could be due to considering the maximum distance between the valley flanks and the inaccurate estimation of the surface of rupture regarding the current exposed part of the scarp. The uncertainty of this approach is also stated in Hermanns et al. (2011a) as nearly 50 %.

2.4. Dam

According to the classification conducted by Tacconi Stefanelli et al. (2015), dam evolution is defined as formed-stable, formed-unstable, and not formed. Formed-stable defines dams that blocked a valley and formed a backwater lake. These dams have not experienced a general failure and all or some parts of them are existing now under stable conditions. Formed-unstable is assigned to the dams which blocked a valley and created a backwater lake for some time (from hours to centuries) until the dam has undergone a failure and the backwater is released downstream of the dam. This class also refers to the dams that are modified by human activities in the form of road construction or stabilization. Not formed is to characterize the landslides that reached the valley and shortened the river bed section, however, the blockage was not enough to form a backwater lake.

The dam type is based on 5 classes defined in Hermanns et al. (2011b): I) Landslide dams formed as depressions on the landslide deposit, II) landslide dams causing single lakes in one valley, III) landslide dams causing multiple lakes in one valley in line, IV) landslide dams at confluences causing multiple lakes in various valleys, V) landslide dam affecting the drainage divide. According to Costa and Schuster (1988), not formed dams are classified as type I.

Dam volume usually has been estimated based on geometric parameters. Although, it is not precise to define the height of the dam only regarding the topographic data since the valley floor before the landslide occurrence is often unknown. According to Curden and Varnes (1996), movements cause volume increase in displaced materials as the result of dilation. For mass-wasting of carbonate rocks, 25–30 % volume increase is reported (Ostermann et al., 2012). Moreover, in a study on landslide dams in the Benner Pass area, Ostermann and Sanders (2017) considered a 10–20 % increase in volume. Thus, the dam volume is approximated by a 10–30 % volume increase in the landslide deposit after detachment from the slope. However, this assumption is not valid for the landslides that spread through more than one valley (for example Tschirgant and
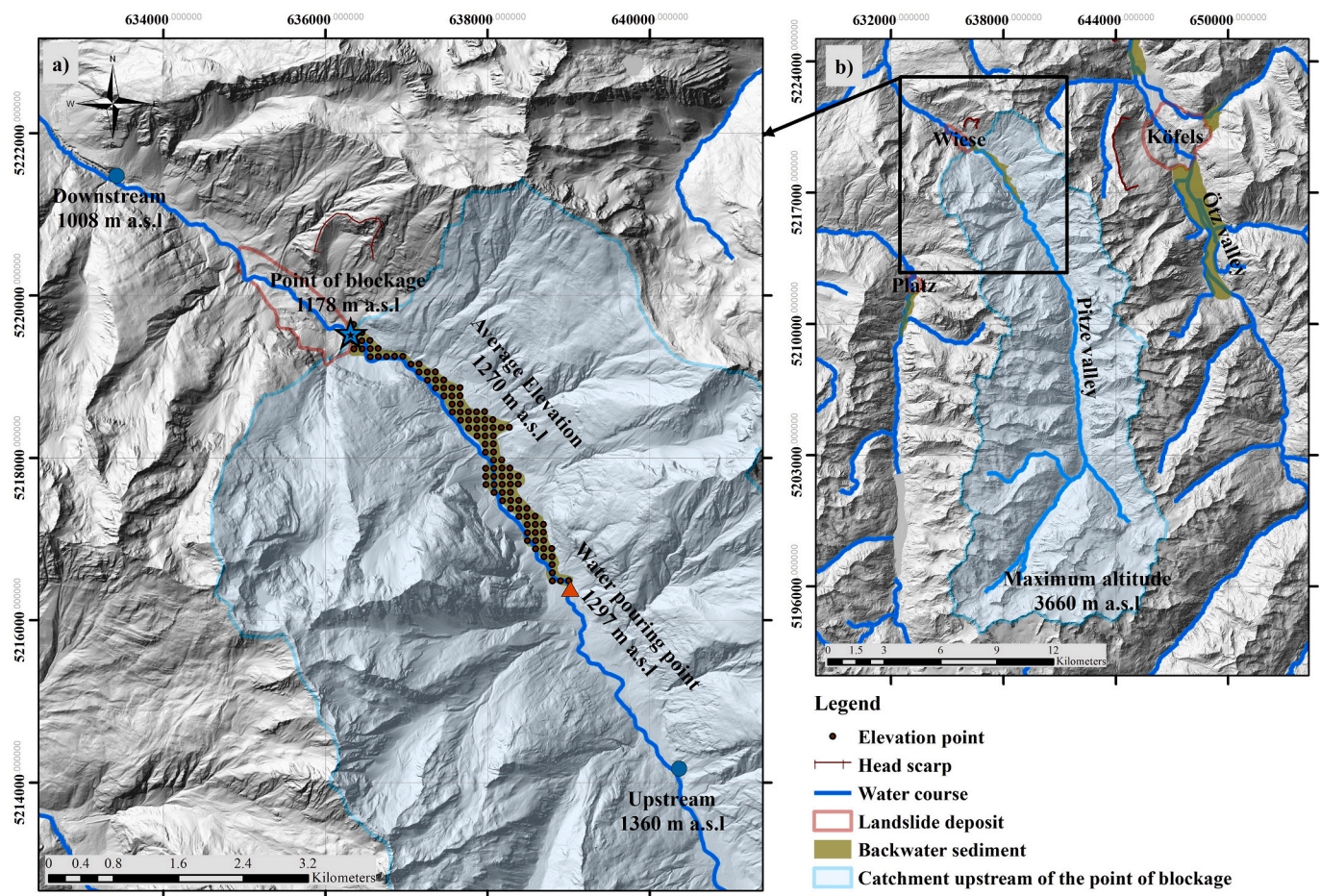
Fig. 5. a) The parameters of the backwater sediments including the water pouring point into the lake, the network of the elevation points, and three reference points (upstream, blockage, and downstream) used for estimation of the channel bed slope, and b) the extent of the catchment upstream of the point of blockage are illustrated on 5 m DEM of Tyrol, Austria (data.gv.at).

Köfels landslides), as the landslide dam comprises parts of the landslide deposit that actively contribute to the blockage process of only one specific valley (Dufresne et al., 2018). Therefore, in such cases, the volume of the landslide dam is less than the total landslide volume. Based on the dam volume estimation, it is possible to calculate the area of the landslide deposit in cross-sections perpendicular to the dammed valley (minimum three to maximum seven based on the dam extension). The average value of the maximum height in these cross-sections is defined here as the mean height of the landslide dam.

The Wiese landslide dam has been widely gone through fluvial incision therefore, its evolution is considered formed-unstable. The landslide deposit once blocked the valley and the materials have transferred fully to the other side of the valley forming a single backwater lake hence, the dam is classified under the type (II) category. Taking a 25 % volume increase, the dam volume is estimated to be 15 Mm^3. Based on the dam extension along the valley (width of the dam is 1.25 km), 5 cross-sections with 300 m spacing perpendicular to the dammed valley are used in the reconstruction of the shape of the valley before the failure of the dam (Fig. 4-a). Given the estimated volume of the landslide accumulation and the spacing between the cross-sections, the area under each cross-section at the location of the dam is determined to obtain the desired volume. Due to the destruction of Wiese dam accumulation, an area above the current topography is assumed as the former landslide deposit (Fig. 4-b). Consequently, the mean height of the dam is calculated based on the defined area in each cross-section at 35 m (Fig. 4-c).

2.5. Lake

Backwater lakes are categorized into three evolution states: (I) existing/partially-filed which relates to the lakes that currently exist upstream of the formed dam or part of the original lake still exists, (II) formed-disappeared which refers to the previously formed lakes that have disappeared through the time, and (III) not formed which is assigned to the landslide dams with no evidence of backwater sediments at their upstream area (Tacconi Stefanelli et al., 2015).

Besides the geometrical parameters, lake mean depth for the formed-disappeared lakes is estimated as the difference between the average elevation inside the determined boundaries and the elevation at the point where the stream is assumed to pour into the lake. Consequently, the lake volume is approximated firstly based on the data provided in the literature and then, on the obtained mean depth and the area of the backwater lake.

The channel bed gradient upstream and downstream of the point of blockage has been calculated based on a constant distance of a reference point in the reviewed literature (Dong et al., 2009). As the length of the formed backwater lakes in this inventory varies in a quite large range (minimum 0.3 km to maximum 11.5 km), the distance in the upstream and downstream of the point of blockage is not considered as a specific value for our cases. To estimate the gradient, the doubled length of the backwater sediment or lake following the streamline is considered as the distance upstream of the point of blockage however, half of this value is specified as the distance downstream of the reference point. Moreover, the mean channel bed slope is also approximated between the defined
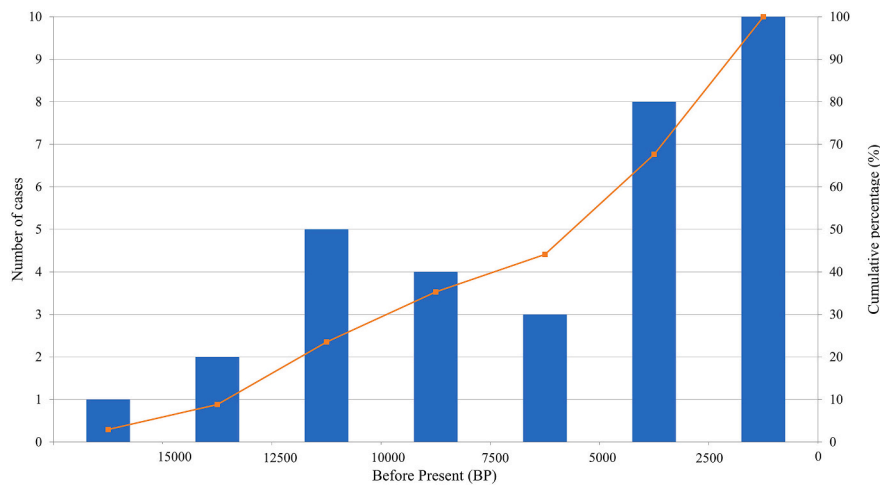
Fig. 6. Temporal occurrence of the landslides archived in the inventory excluding two Pleistocene landslides i.e. Butterbichl (114–113 ka) and Mariastein (minimum 62–68 ka). Time 0 in the x-axis is 1950 CE.

points (Fig. 5-a). For the cases where the catchment upstream of the point of blockage is smaller than the double length of the backwater sediment or lake, the gradient is calculated at the catchment border.

Since only backwater sediments can be tracked upstream of the Wiese landslide deposit, the lake is assumed formed-disappeared. The average elevation inside the lake boundaries is estimated by developing a 100 m spacing network of the elevation points. Given the average elevation of 1270 m a.s.l. and the pouring point elevation of 1297 m a.s. l. (Fig. 5-a), the mean depth of the Wiese backwater lake is approximated 27 m. Considering the 3.85 km length of the Wiese backwater sediments, two reference points are identified downstream and upstream of the point of blockage following the streamline. The mean, upstream, and downstream gradients then are estimated based on the obtained elevations and the horizontal distance between these points as 0.035, 0.027, and 0.049, respectively.

2.6. Catchment

Catchment parameters are defined based on the point of blockage for the formed-stable and formed-unstable dams. Moreover, it is possible to determine these parameters for the not-formed dams in which a point of blockage can be identified. The watershed is specified at the reference point through a hydrological analysis in Arc-GIS. Relief is defined as the elevation difference between the highest and lowest points in a watershed (Patton, 1988), however, to adjust this term in the context of landslide dams, Korup (2004) took the lowest altitude of the catchment as the difference of the dam crest elevation and the dam height. The Melton ruggedness number is a dimensionless flow accumulation index of the basin (Melton, 1965). It combines the steepness and the extent of the catchment to discriminate basins with debris flow potential from basins in which the bedload counts as the dominant factor in the sediment transport process (Marchi and Dalla Fontana, 2005).

The Wiese landslide accumulation blocks the Pitze river at the elevation of 1178 m a.s.l. Based on the Arc-GIS hydrological analysis, the watershed upstream of the point of blockage extends about 213.50 km^2 reaching 3660 m a.s.l. elevation (Fig. 5-b).

3. Results

3.1. Database description

The presented landslide dam database geographically covers Austria (46 %), Italy (44 %) and Germany (10 %).

The total number of 53 rivers is recognized as the related stream during the formation of the dam. Between the detected waterways, Inn and Ötztaler Ache each have been blocked 5 times by different landslide deposits, followed by Torrente Avisio dammed in 4 spots. The largest extent of the catchment area is observed on Inn river as the result of Pletzachkogel landslide occurrence.

The age of the landslides as a specified estimated value was only available for 35 cases of the inventory. A high range of timeline from 113 to 114 ka (thousand years ago) for Butterbichl landslide dam in Tyrol, Austria (Gruber et al., 2009; Starnberger et al., 2013), to 1950 CE (common era) for Forcelles landslide in South Tyrol, Italy (Stuiver and Reimer, 1993) is covered by the presented numbers. According to Fig. 6, about 85 % of the dated events occurred during the Holocene era. Besides, the age of the few landslides such as Ehrwald (Prager et al., 2008), Lienzer Klause and Mordbichel (Reitner et al., 2014) in Tyrol, Austria are stated in the literature as Holocene and late Holocene, respectively. About 60 % of the landslides that occurred in the Holocene age are dated 0 to 5000 BP which shows a time lag of several thousand years between deglaciation and slope collapses. Therefore, the landslide activities in the Holocene age are assumed dependent on the climate fluctuations (Prager et al., 2008).

A cluster of large landslides is detected in Tyrolean Alps (Fernpaß area, Inn valley, and Ötz valley) between 3.0 and 4.2 ka BP. These events indicate climatic phases of increased water supply as they temporally equated with the progradation of some larger debris flows in the nearby main valleys, and partially, with glacier advances in the Austrian Central Alps (Prager et al., 2008). A rather smaller cluster is also observable at the location of the Sterzing basin between 11.2 and 13.6 ka BP. These landslides likely occurred during the Younger Dryas climatic phase in which the source areas of the catastrophic rock-slope failures were free of glacial ice. Although a specific paleoclimatic condition is not assigned to these landslides, meteorological situations such as short-term heavy rainfall can be accounted as the triggering factor (Ostermann and Sanders, 2017).

In the current inventory, the formed-stable and formed-unstable classes each hold 45 % of the cases while the not-formed dams comprised only 10 % of the database. Overall 82 % of these landslide dams are categorized as type II. However, type I and type IV each represent 11 % and 7 % of the data. Two blockage types of III and V have not been recognized in any cases of this inventory. The dominant blockage type agrees with both Northern Apennines (Casagli and Ermini, 1999) and Italian (Tacconi Stefanelli et al., 2015) databases. Meanwhile, type I with 11 % is much less in comparison to these two inventories (19 % in Northern Apennines and 27 % in Italy) which is due to the lower number of not-formed dams in the study area region. As
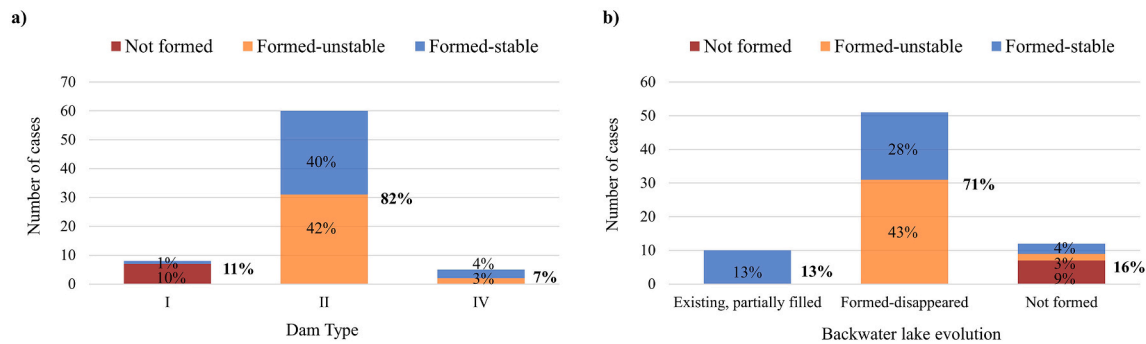
Fig. 7. a) Dam evolution classification based on the type of the dams for 73 cases. Among the defined categories in Hermanns (2013), three types of I, II, and IV are distinguished in the database while the most frequent type is identified as II. b) The evolution state of 76 backwater lakes is shown based on the dam's evolution.

Table 1
Statistical analysis of the geometric parameters of the developed landslide dam database.

	Geometric parameter	Minimum	Maximum	Mean	Standard deviation	Median	Skewness	Kurtosis	Number of cases
Landslide	Height (m)	145.0	2120.0	879.1	402.4	880.0	0.5	0.1	73
	Runout angle (°)	5.2	43.8	19.1	7.1	18.5	0.7	1.2	73
	Runout length (km)	0.7	15.5	3.0	2.3	2.4	2.9	12.6	73
	Volume (Mm^3)	0.5	3200.0	99.6	391.9	15.0	7.2	56.5	73
Dam	Area (km^2)	0.04	12.9	1.4	2.1	0.6	3.3	13.7	72
	Length (km)	0.1	15.4	1.1	1.9	0.6	6.6	50.4	72
	Width (km)	0.2	6.0	1.7	1.1	1.3	1.6	3.0	72
	Mean height (m)	5.0	450.0	57.8	60.0	45.0	4.2	25.8	71
	Volume (Mm^3)	0.6	2164.0	91.9	290.7	17.0	6.0	39.2	72
	Dam crest elevation (m a.s.l.)	520.0	2145.0	1321.9	425.0	1330.0	0.0	−1.0	71
	Width of the dammed valley (km)	0.1	5.3	0.8	1.0	0.5	2.9	9.7	73
Lake	Area (km^2)	0.02	22.6	2.1	4.0	0.6	3.2	11.6	64
	Length (km)	0.3	11.5	3.0	2.6	1.9	1.6	2.3	64
	Width (km)	0.1	4.0	0.8	0.8	0.5	2.3	5.2	64
	Mean depth (m)	2.0	84.0	21.8	18.4	16.0	1.6	2.6	64
	Volume (Mm^3)	0.2	897.3	47.3	130.5	10.2	5.2	30.4	64
	Mean channel bed slope (m/m)	0.0	0.2	0.1	0.1	0.1	1.0	0.7	64
	Upstream channel bed slope (m/m)	0.0	0.3	0.1	0.1	0.1	1.5	2.1	64
	Downstream channel bed slope (m/m)	0.0	0.3	0.1	0.1	0.0	1.8	3.4	64
Catchment	Area (km^2)	1.9	8508.8	507.6	1348.0	51.7	4.3	20.2	73
	Maximum altitude (m a.s.l.)	680.0	4020.0	2920.8	584.6	2925.0	−0.9	2.2	73
	Relief (m)	70.0	3335.0	1703.7	687.5	1618.0	0.4	−0.2	73
	Relief ratio (m/km^2)	0.2	508.7	56.3	77.5	31.5	3.3	15.8	73
	Mean slope (°)	5.0	40.0	27.2	4.9	30.0	−1.5	5.6	73
	Melton ruggedness number	0.02	0.6	0.2	0.1	0.2	0.6	0.0	73

shown in Fig. 7-a, dam type I constitutes mainly of not formed cases and only one formed-stable landslide dam, Buchwiese (Reitner et al., 2020), in which the dam was formed on the landslide deposit depressions.

The formed lake upstream a landslide deposit acts as a driving force jeopardizing the stability of the dam hence, classifying the evolution of the backwater lakes is functional for distinguishing stable dams out of unstable ones. The majority of the backwater lakes in the current inventory are classified as formed-disappeared (71 %) while only 16 % of the formed lakes are still completely or partially existing and for 13 % of the dams, no backwater lake was formed at all. In Fig. 7-b, the evolution of the backwater lakes is shown based on the corresponding dam evolution. Out of 71 % of the formed-disappeared dams, 43 % are accompanied by a formed-unstable case indicating the dam failure and consequently the destruction of the lake. On the other hand, the formed dams in 28 % of the formed-disappeared lakes are considered stable which suggests the filling of the backwater lake with sediments through time. No backwater lake can be formed upstream of the not formed dams, as they only reduce the river bed section. In a few cases, no backwater lake was formed upstream of a formed dam (7 %) which could be due to several different morphological reasons, e.g. porosity. As an example, the Tschirgant landslide which is archived as formed-unstable, blocked both Inn and Ötztaler Ache rivers but, since the backwater area in the Inn valley lies within and beyond a narrow

bedrock gorge, no trace of sediments has been found upstream of the Inn valley (Dufresne et al., 2018).

3.2. Statistical analysis of the geomorphic parameters

Besides the qualitative parameters of the inventory, a geometrical characterization requires a statistical analysis of the dataset (Table 1). The difference between maximum and minimum in some parameters such as catchment area indicates the high diversity of values relating to the geomorphic conditions. The highest catchment area value (8508.8 km^2) is assigned to the Pletzachkogel landslide blocking the Inn river at the far most spot from its source while the Hallthurm Landslide by damming the 10 km length Rötelbach river, is being exposed to a 1.9 km^2 watershed. The difference between the mean and median in these skewed parameter distributions lead to high skewness and kurtosis points. The mean value for the catchment area is stated 507.6 km^2 however, for 62 % of the data, the watershed is calculated as <100 km^2. Extreme high numbers of skewness (over 5) and kurtosis (over 30) in the parameters such as landslide volume, dam length, dam volume, and lake volume indicate the existence of outliers in comparison to the mean value. This can also be evidenced regarding the unique cases in the inventory. As an example, the volume of Köfels landslide (3200 Mm^3) as the second-largest landslide in the entire Alps differs largely from the

Table 2

Comparison between the representative parameters of the presented database and other landslide dams' inventories.

Location	Landslide volume (Mm³)		Dam volume (Mm³)		Dam height (m)		Lake volume (Mm³)		References
	Mean	Number of cases	Mean	Number of cases	Mean	Number of cases	Mean	Number of cases	
Part of the Eastern Alps	100	73	92	72	58	71	47	64	This study
Argentina	339	45	–	–	92	43	–	–	Hermanns et al. (2011a)
Italy	24	263	4	260	23	259	15	62	Tacconi Stefanelli et al. (2015)
Japan	14	43	3.6	43	51	43			Dong et al. (2009)
New Zealand	–	–	303	118	67	118	73	87	Korup (2004)
Worldwide	–	–	79	84	53	84	–	–	Ermini and Casagli (2003)

Table 3

Correlation matrix of the geomorphic parameters of the presented database.

mean value (almost 100 Mm³).

To compare the estimated values in this database with other inventories, the mean value of representative parameters of landslide, dam, and lake are presented in Table 2. The mean landslide volume of the presented database (100 Mm³) is much higher than the mean of 263 cases in the Italian (24 Mm³) and 43 cases in the Japanese databases (24 Mm³) due to the existence of some large landslides in the former such as Köfels (3200 Mm³) and Fernpaß (1000 Mm³) while the volume of the largest landslide in the Italian and Japanese inventories are about 300 and 130 Mm³, respectively. Even though the largest landslide in the Argentinian database (3100 Mm³) is compatible with the Köfels in Eastern Alps, the mean value is >3 times higher than the one from the part of Eastern Alps as the result of encompassing a few more large landslides (larger than 1000 Mm³). The range of the dam volume of the presented data inventory is relatively compatible with the worldwide database. On the other hand, the mean dam volume of the New Zealand database is much higher than for the part of Eastern Alps and for the worldwide inventories because of the 27,000 Mm³ deposit of the huge Green lake landslide dam. Identically, the mean lake volume of the New Zealand inventory is larger than the one in the part of the Eastern Alps

database. Despite the high difference between the largest lakes in two of the databases (5000 Mm³ backwater lake - Green lake landslide dam, New Zealand and almost 900 Mm³ Sterzing backwater lake - Stilfes landslide dams, Pfitsch, Wipp, and Ridnaun valleys, South Tyrol, Italy) the difference seems reasonable. The dam mean height of the part of Eastern Alps, Japan, New Zealand, and worldwide datasets varies in an almost 15 m range indicating a close estimation in different geographical regions. Normally, including larger landslides, the Argentinian database presented a deeper dam mean height than the rest of the inventories. Accordingly, the dam mean height of the Italian cases is almost half of the dominant range (51 to 67 m) due to comprising of relatively smaller landslide dams.

Due to the dependency of the geomorphic parameters on one another, their correlation as a statistical approach would lead to discerning geomorphic relationships. Here, Pearson's product-moment correlation coefficient for two sets of data is used to measure the strength and direction of a linear association between two variables (Pearson, 1948). The coefficient is denoted by r:

$$r = \frac{S_{xy}}{S_x S_y} \qquad (2)$$

where S_{xy} is the covariance, S_x and S_y are the standard deviation of x and y, respectively. Correlation coefficient r can have a value between -1 and 1 where the positive and negative ones exhibit uphill and downhill relation of two sets of data, respectively. A perfect linear relationship is obtained at $|r| = 1$, $0.8 < |r| < 1$ indicates a fairly strong correspondence, $0.6 < |r| < 0.8$ defines a moderate connection, $0 < |r| < 0.6$ stands for a weak association, and 0 shows a nonlinear relationship. In Table 3 the correlation matrix of the geomorphic parameters is presented for the variables indicating at least one correlation coefficient equal or >0.6. Except for the cells showing the relation between the same categories, the bold numbers represent a fairly strong positive relationship of the variables (r > 0.8). The geometric parameters of the landslide and dam show the best correlation as the runout length of the landslide is strongly correlated with the area and length of the dam. The volumes of the dam and landslide indicate the highest correlation coefficient (0.9) due to the estimation of the landslide deposit volume as a percentage of the landslide volume. However, the dam height approximated based on the perpendicular cross-sections on the dammed valley is also fairly strong correlated (0.8) with the landslide volume. The physical parameters of the lake such as area and width are being affected by the width of the dammed valley, although no other strong correlation with either dam or landslide parameters has been detected. Among the geomorphic parameters of the lake and the upstream catchment area, no strong correlation is observed. Though, moderate correlations exist between the area of the catchment upstream of the point of blockage and both area and width of the lake. On the other hand, the Melton ruggedness number shows only a positive moderate correlation with the channel bed slope as it is defined regarding the steepness of the catchment upstream of the point of blockage. The overall observation of the correlation matrix specifies the statistical dependency of the landslide and dam geomorphic parameters on one another, nonetheless, the catchment area and the formed lake are statistically independent of the landslide parameters.

3.3. Stability assessment of landslide dams using geomorphic indices

Geomorphic indices are accounted as a reliable predictor in assessing the stability of the landslide dams. To evaluate the applicability of the developed indices in the literature on the presented data inventory, the dam stability and lake availability plots are provided. To distinct stable and unstable domains on these plots, the separating bounds are estimated as 95 % confidence interval of the index mean value instead of considering the absolute maximum and minimum values as the lower and upper bounds despite the literature. As the result of the definition of the bounds, and regarding the distance between the mean values of the data, an area is formed between lower and upper bounds as the uncertain domain in which the stability of the cases is not anticipated by the geomorphic index. A summary of the defined bounds and the percent of the data within the uncertain domain for the geomorphic indices which are used in this study is presented in Table B.1. Consequently, the comparisons in the following section are based upon the obtained statistical bounds and these absolute ones.

The geomorphic indices are usually developed based on only a few characteristics of the complex system of a landslide dam. Hence, it is always probable that a landslide dam behaves differently than what is predicted by the geomorphic index. Thus, applying the statistical approach decreases the effects of the exceptional cases in defining the main domains and makes the bounds more flexible in case of implementing other geographical regions or future cases. However, the statistical approach makes the presence of the outliers in the established domains inventible. Outliers are referred to the cases that despite their evolution state, lay inside the opposite defined domain. In the assessment of the applicability of the geomorphic indices on the developed

inventory, the percent of data in the uncertain domain and the number of outliers counted as our criteria. The size of the uncertain domain can only be compared with the literature. However, a limit for the number of outliers in each graph is set which is identical to 5 % of the whole data. If the number of outliers exceeds the limit, the index would count as inapplicable. It should be also noted that due to the insufficient data for the existing, partially filled lakes in the database, the obtained bounds cannot be presented as solid results. Therefore, the only presented bound for the lake availability plots is the upper bound of the formed-disappeared lakes.

3.3.1. Blockage index

Canuti et al. (1998) proposed a revised version of the theory of Swanson et al. (1986) which is based on the dependence of the landslide dam stability on the relation of the landslide volume and the area of the watershed upstream of the point of blockage in the form of a blockage index BI:

$$BI = log\left(\frac{V_d}{A_c}\right) \qquad (3)$$

where V_d [m^3] is the volume of the landslide deposit that blocks the valley and A_c [km^2] is the area of the catchment upstream of the point of blockage. Plotting the data based on the dam evolution results in an unstable domain for BI < 4.6, and a stable domain for BI > 6.2 (Fig. B.1-a). The blockage index is also applied based on the existence or failure of the backwater lakes (Korup, 2004; Fig. B.1-b). The cases holding BI < 5.0 have disappeared through time which agrees with the New Zealand database where unstable lakes have shown BI < 4.0 (Korup, 2004).

3.3.2. Impoundment index

The impoundment index I_i has been developed by Casagli and Ermini (1999):

$$I_i = log\left(\frac{V_d}{V_L}\right) \qquad (4)$$

where V_d [m^3] is the volume of the landslide deposit and V_L [m^3] is the backwater lake volume. Applying this index on the presented inventory, a stable domain is obtained for $I_i > 0.8$ and an unstable domain for $I_i < -0.3$ (Fig. B.2-a). The high number of outliers (11 % of the whole data) shows the inefficiency of the impoundment index in distinguishing stable and unstable cases. On the other hand, the formed-disappeared lakes are effectively clustered under $I_i = 0$ (Fig. B.2-b). In a study conducted by Korup (2004) on the New Zealand landslide dam database, the $I_i > 1$ is set as an absolute lower bound for existing lakes. Therefore, the obtained results of two inventories complete one another.

3.3.3. Dimensionless blockage index

Considering the influence of the landslide dam height on the global stability of the dam, Ermini and Casagli (2003) proposed a dimensionless blockage index DBI:

$$DBI = log\left(\frac{A_c H_d}{V_d}\right) \qquad (5)$$

where V_d [m^3] represents the volume of the landslide deposit that blocks the valley, H_d [m] the dam height, and A_c [km^2] the area of the catchment upstream of the point of blockage. The formed-unstable cases in the part of the Eastern Alps database have shown a DBI > 2.8 (Fig. B.3-a) which corresponds with the 2.68 to 3.23 range stated in Ermini and Casagli (2003). The upper bound determining the formed-stable dams is DBI < 1.5 which is not in complete agreement with the 2.68 to 2.83 range stated in Ermini and Casagli (2003). Nevertheless, the variability of the 36 Italian and Alps cases in the mentioned inventory is quite low. Hence, as the result of adding more cases and using a constant data gathering method, the variability has increased in the presented

database which leads to a slight change in the obtained upper bound. The DBI has also been applied to the Italian database (Tacconi Stefanelli et al., 2016) obtaining an uncertain domain between 2.43 and 3.98 that covers 76 % of the data. However, the uncertain domain for the part of Eastern Alps inventory is about 60 %. Use of the index to set a bound for the formed-disappeared lakes yields a DBI > 2.5 (Fig. B.3-b) while the stated bound in the New Zealand database is 3 (Korup, 2004). Though, if the minimum value of the existing, partially filled lakes was considered as the lower bound, the same DBI = 2.9 as the previous research results would be obtained.

3.3.4. Backstow, basin, and relief indices

In a study conducted by Korup (2004), three dimensionless indices have been proposed which employed the landslide dam height as the main resisting factor towards instability. The backstow, basin and relief indices are defined as follows:

$$I_s = log\left(\frac{H_d^3}{V_L}\right) \tag{6}$$

$$I_a = log\left(\frac{H_d^2}{A_c}\right) \tag{7}$$

$$I_r = log\left(\frac{H_d}{H_R}\right) \tag{8}$$

where H_d is the landslide dam height [m], V_L is the volume of the lake [m^3], A_c [km^2] and H_R [m] are the area of the catchment and the relief upstream of the point of blockage. Applying the backstow index on the part of the Eastern Alps database results in a stable domain with $I_s > -1.3$ and an unstable domain with $I_s < -3.2$ (Fig. B.4-a). The defined range of the uncertain domain in the original work is between 0 and −3 which is compatible with the upper bound of the unstable domain here, however, the stable lower bound is set much lower. The difference between the limits is due to the difference in the mean value of the dam height in the two data inventories. Generally, the existence of 6 outliers (nearly 9 % of data) indicates a weak separation between the stable and unstable cases of the current database depending on the backstow index. On the other hand, the formed-disappeared lakes are separated showing a low number of outliers (2) at $I_s < -2.7$ (Fig. B.4-b).

The use of the basin index on the presented database yields a stable domain for $I_a > 2.3$ and an unstable domain for $I_a < 0.4$ (Fig. B.5-a). Due to the high number of outliers (7 % of data), the basin index is not particularly sufficient in separating the stable and unstable domains. The index was initially developed to set a bound for the existing lakes ($I_a > 3.0$). Regarding the accessible data, $I_a < 0.9$ defines the upper bound of the formed-disappeared lakes (Fig. B.5-b). Even though the obtained bound is not comparable to the original one, it shows no contradiction towards that.

Implementing the relief index on the part of the Eastern Alps database yields in a stable domain with $I_r > -1.3$ and an unstable domain with $I_r < -1.9$ (Fig. B.6-a). However, regarding the existence of 6 outliers (9 % of the whole data), relief height is not constructive in defining the domains. Same as the basin index, the relief index is also suggested to distinct existing lakes ($I_r > -1$). According to the developed inventory, the formed-disappeared lakes have shown $I_r < -1.8$ and the rest is uncertain (Fig. B.6-b).

3.3.5. Hydromorphological dam stability index

Relying mostly on the effects of the landslide volume in the geomorphological evolution of the landslide dams, Tacconi Stefanelli et al. (2016) suggested the hydromorphological dam stability index HDSI as follows:

$$HDSI = log\left(\frac{V_l}{A_C \times S}\right) \tag{9}$$

Table 4
Summary of the application of the existing geomorphic indices on the part of Eastern Alps database.

Index	Domain	Index bound	Data within the bound (%)	Data within the uncertain domain (%)	Number of outliers
BI	Stable dam	BI > 6.2	14.7	64.7	3
	Unstable dam	BI < 4.6	20.6		
	Formed-disappeared lake	BI < 5.0	35.9	64.1	1
I_i	Stable dam	I_i > 0.8	15.6	65.6	7
	Unstable dam	I_i < −0.3	18.8		
	Formed-disappeared lake	I_i < 0	37.5	62.5	2
DBI	Stable dam	DBI < 1.5	19.1	60.3	4
	Unstable dam	DBI > 2.8	20.6		
	Formed-disappeared lake	DBI > 2.5	37.5	62.5	1
I_s	Stable dam	I_s > −1.3	18.8	60.9	6
	Unstable dam	I_s < −3.2	20.3		
	Formed-disappeared lake	I_s < −2.7	32.8	67.2	2
I_a	Stable dam	I_a > 2.3	17.6	64.8	5
	Unstable dam	I_a < 0.4	17.6		
	Formed-disappeared lake	I_a < 0.9	32.8	67.2	0
I_r	Stable dam	I_r > −1.3	14.7	67.6	6
	Unstable dam	I_r < −1.9	17.7		
	Formed-disappeared lake	I_r < −1.8	32.8	67.2	2
HDSI	Stable dam	HDSI > 7.2	12.5	67.2	8
	Unstable dam	HDSI < 6.2	20.3		
	Formed-disappeared lake	HDSI < 6.4	31.3	68.7	3

where V_l is the landslide volume [m^3], A_c is the area of the catchment upstream of the point of blockage [km^2], and S is the channel bed slope [–]. Applying the HDSI on the developed data inventory yields in the stable domain of HDSI > 7.2 and the unstable domain of HDSI < 6.2 (Fig. B.7-a). The stable lower bound is compatible with the 7.44 absolute bound stated in the original work. However, the unstable upper bound is higher than the 5.74 absolute instability domain of the Italian database due to the higher mean value of the landslide volume in the part of the Eastern Alps data inventory (Table 2). Moreover, the percent of data in the uncertain domain is comparable to the value in the original main work (67.2 % here in comparison to 66 %). The HDSI also applied on a set of Peruvian landslide dams which results in a wider uncertain domain than Italian and part of Eastern Alps databases (72 %). Still, because of the high number of outliers (12 % of whole data), HDSI is not evaluated as a sufficient index to disparate the stable and unstable domains of the part of the Eastern Alps database. Considering backwater lakes, formed-disappeared cases show HDSI < 6.4 with only 4 % of the data as outliers (Fig. B.7-b).

Applying the existing geomorphic indices on the part of Eastern Alps data inventory yields in a variety of bounds indicating domains for the
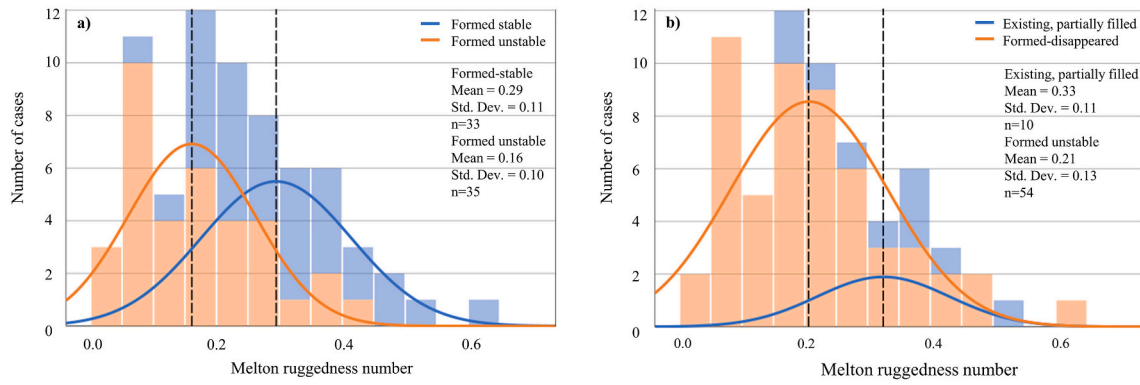
Fig. 8. Stacked histograms of Melton ruggedness number by (a) dam evolution and (b) lake evolution. The mean value of each group is portraited by a dashed line.

stable and unstable dams as well as lower bound of the formed-disappeared lakes. Since the bounds are determined based on a 95 % confidence interval of the mean value of each category, a measure for the quality of the mean value calculation can be given. The amount of the data within the defined bounds, the range of the uncertain domain, and the number of outliers declare the applicability of the indices on the data inventory. As it is summarized in Table 4 the uncertain domain

varies between almost 60 to 69 %. Dimensionless blockage index, by showing a 60.3 % uncertain domain and 4 outliers, separates the stable and unstable domains of the part of the Eastern Alps database better than the other indices. Moreover, the blockage index by holding 64.7 % of the data in the uncertain domain and 3 outliers, stands as an applicable index on our data inventory. On the other hand, all of the indices are applicable for distinguishing the formed-disappeared lakes as the
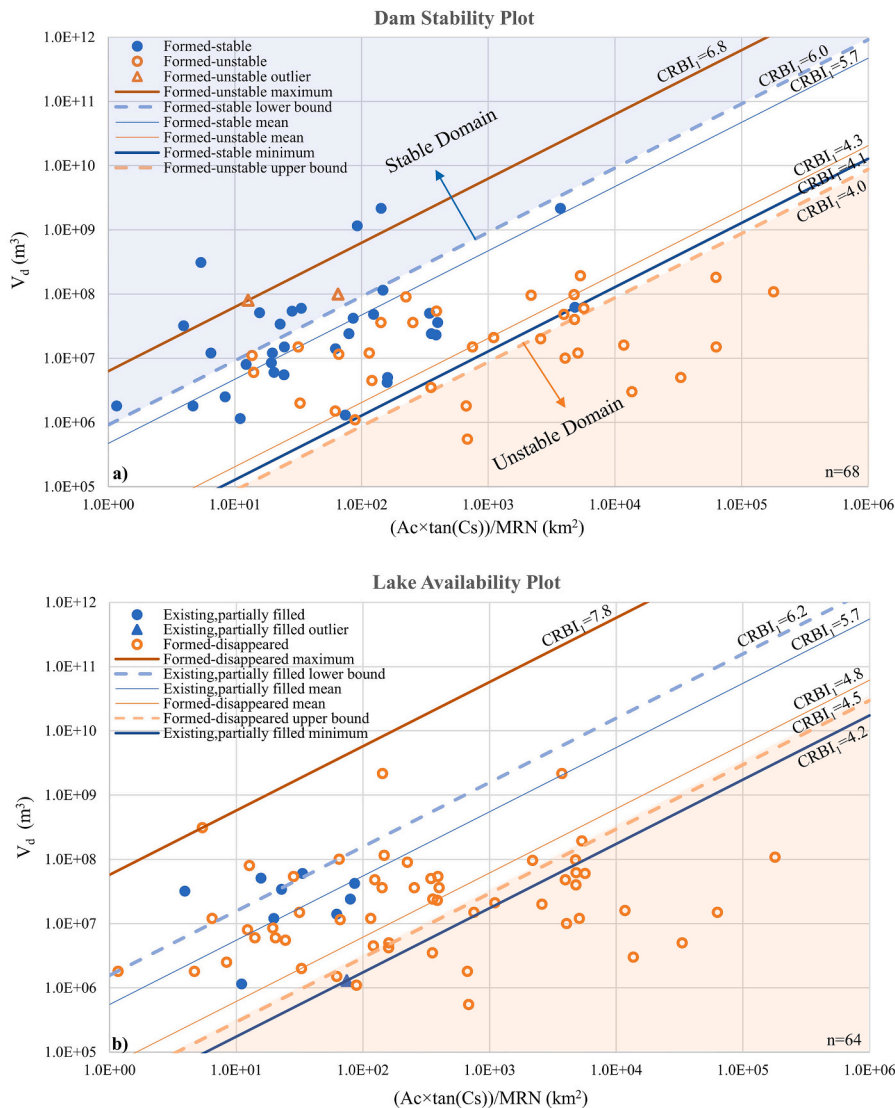
Fig. 9. (a) Dam stability plot of the part of Eastern Alps inventory based on CRBI1. Blue lines show results for stable cases, and orange lines show the results for unstable cases. The mean values are plotted with thin lines. For the stable cases, the minimum value is plotted with a thick blue line while for the unstable cases, the maximum value is shown as a thick orange line. The blue and orange dashed lines indicate the lower bound of the stable cases (95 % confidence level upper than the mean) and the upper bound of the unstable cases (95 % confidence level lower than the mean), respectively. (b) Lake availability plot of the part of the Eastern Alps inventory based on the CRBI1. Blue lines show results for the existing, partially filled cases, and orange lines show the results for the formed-disappeared cases. The mean values are plotted with thin lines. For the existing, partially filled cases the minimum value is plotted with a thick blue line while for the formed-disappeared cases the maximum value is shown as a thick orange line. The blue and orange dashed lines indicate the lower bound of the existing, partially filled cases (95 % confidence level upper than the mean) and the upper bound of the formed-disappeared cases (95 % confidence level lower than the mean), respectively. (For interpretation of the references to color in this figure legend, the reader is referred to the web version of this article.)
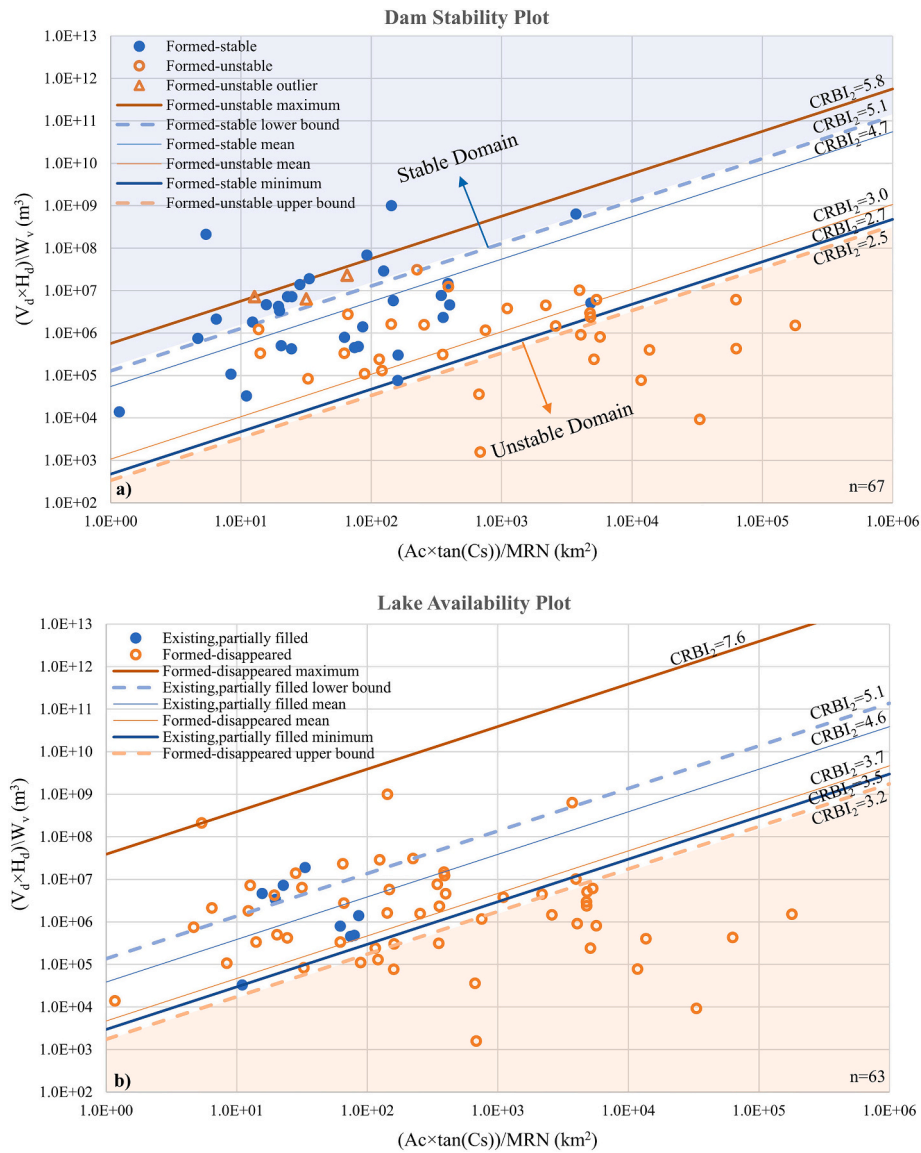
Fig. 10. (a) Dam stability and (b) lake availability plots of the part of the Eastern Alps inventory based on the CRBI$_2$.

number of the outliers has not exceeded the set threshold (5 % of the whole data). Dimensionless blockage index and impoundment index including 37.5 % of data within the defined bounds have shown the best relevancy followed by the blockage index encompasses 35.9 % of the data under the set bound.

3.4. Catchment ruggedness-based indices

The logic behind the geomorphic indices defining the stable and unstable domains is based on the relation of the resisting and driving forces affecting the formed dam and backwater lake. In the reviewed state of the art, the significant effect of the representative parameters of the catchment upstream of the point of blockage on the longevity of the formed lakes and the stability of the dams is neglected. Besides the area of the watershed, the mean slope of the catchment defines the sediment dynamics; the higher the catchment slope, the higher the dynamics of the sediments. However, a solid statement cannot be assigned to the Melton ruggedness number as it depends on the steepness of the catchment as well as the reverse square root of its area. As presented in Fig. 8, the statistical process of the current data inventory has shown a smaller mean value of the Melton ruggedness number for the unstable

dams (0.16) and the formed-disappeared lakes (0.21) compared to the stable dams (0.29) and the existing, partially filled lakes (0.33).

Three new geomorphic indices named catchment ruggedness-based indices (CRBI) are presented in this study sharing the same driving force as a function of the catchment area, the catchment mean slope, and the Melton ruggedness number. The resisting forces are different for each index and are based on the dominant characteristics of the formed dam and the responsible landslide:

$$CRBI_1 = log\left(\frac{V_d}{(A_c \times tan(C_s)/MRN}\right) \tag{10}$$

$$CRBI_2 = log\left(\frac{(V_d \times H_d)/W_v}{(A_c \times tan(C_s)/MRN}\right) \tag{11}$$

$$CRBI_3 = log\left(\frac{(H_d \times R_L)}{(A_c \times tan(C_s)/MRN}\right) \tag{12}$$

where V_d [m^3] is the landslide dam volume, A_c [km^2] the catchment area upstream of the point of blockage, C_s the mean slope of the catchment, MRN the Melton ruggedness number, H_d [m] the mean height of the dam, W_v [m] the width of the dammed valley, and R_L [m] the runout
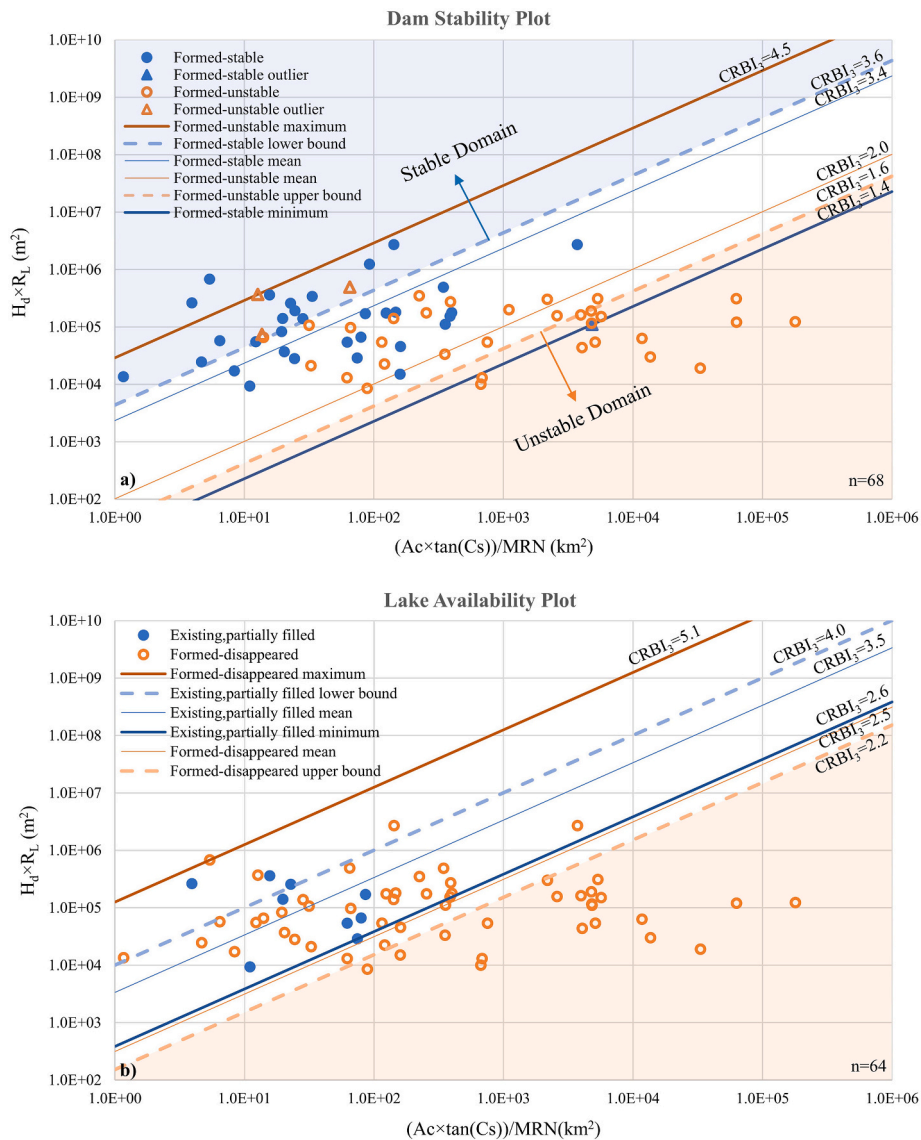
Fig. 11. (a) Dam stability and (b) lake availability plots of the part of the Eastern Alps inventory based on the CRBI₃.

length of the landslide. The width of the dammed valley has been applied previously in an index developed by Tacconi Stefanelli et al. (2016) (Morphological obstruction index) as a reversed effective parameter on the formation of the dams. In the developed dataset, the mean width of the dammed valleys for unstable dams is two times larger than the width of valleys containing stable dams. Therefore, W_v shows an inverted relation with the stability of the landslide dams. The runout length indicates a fairly strong correlation with the area and length of the dam. However, the amount of material spread without considering the mean height of the dam would not be a representative factor of the stability. Due to the higher mean value of the runout length in the stable dams (mean = 3.1 km) than the unstable ones (mean = 2.8 km), its relation with the stability of the dam is considered straight.

Applying the developed indices on the part of Eastern Alps inventory yields in a stable domain for CRBI₁ > 6, CRBI₂ > 5.1, and CRBI₃ > 3.6. The upper bounds for the unstable domains are CRBI₁ < 4, CRBI₂ < 2.5, and CRBI₃ < 1.6 (Figs. 9-a, 10-a, and 11-a). Despite increasing the number of outliers from CRBI₁ to CRBI₃ (2, 3, and 4, respectively), the trend of the bounds confirms a decreasing uncertainty domain from the first index to the last one: 67 %, 61 %, and 59 % respectively. CRBI₂ stands as the index that separates the stable dams at the highest rate (22.4 %). Although, unstable dams are distinguished most effectively

(20.6 %) by CRBI₃. Considering lake availability, the upper bounds of the formed-disappeared lakes are CRBI₁ < 4.5, CRBI₂ < 3.2, and CRBI₃ < 2.2 (Figs. 9-b, 10-b, and 11-b). CRBI₃ performs slightly more functional than other indices including 33 % of data within the defined bound without showing any outlier nevertheless, CRBI₁ and CRBI₂ follow closely keeping 33 % and 32 % of data under the set bound and showing 1 outlier in CRBI₁ (Table 5). Despite the different rate of separation and number of outliers, the defined geomorphic indices are effectively applicable in defining specific domains regarding the normal distinct distribution of the stable and unstable dams and the formed-disappeared lakes (Fig. 12). Indeed, the cumulative frequency trend of each set of data in Fig. 13 displays the separation of the groups with the increase in the number of the data.

3.4.1. Linear modeling algorithms of the catchment ruggedness-based indices

Evaluation of the prediction function of the input parameters (predictors) on each developed geomorphic index (target) is modeled by a linear regression y (IBM, 2015):

$$y = Xb + e \tag{13}$$

Table 5

Performance of the CRBI developed based on the part of the Eastern Alps landslide dam inventory.

Index	Domain	Index bound	Data within the bound (%)	Data within the uncertain domain (%)	Number of outliers
$CRBI_1$	Stable dam	$CRBI_1 > 6.0$	14.7	67.6	2
	Unstable dam	$CRBI_1 < 4.6$	17.7		
	Formed-disappeared lake	$CRBI_1 < 4.5$	32.8	67.2	1
$CRBI_2$	Stable dam	$CRBI_2 > 5.1$	22.4	61.2	3
	Unstable dam	$CRBI_2 < 2.5$	16.4		
	Formed-disappeared lake	$CRBI_2 < 3.2$	31.7	68.3	0
$CRBI_3$	Stable dam	$CRBI_3 > 3.6$	20.6	58.8	4
	Unstable dam	$CRBI_3 < 1.6$	20.6		
	Formed-disappeared lake	$CRBI_3 < 2.2$	32.8	67.2	0

where e follows a normal distribution (mean 0 and variance D^{-1} (D^{-1} = diag($1/g_1$, …, $1/g_n$))) and b is computed applying the sweep operation on a weighted sample correlation matrix R. R is constructed first of the weighted sample means, variances, and covariances among X_i, X_j, I, j = 1…, p, and y, and second of the computed weighted sample correlations r_{ij}. By repeating the sweep operations on each row of the matrix, the last column ($\tilde{r}_{yy}$) contains the standardized coefficient estimates where the singularity tolerance of the model is set 1^{-12} as the result of including all the predictors in the model. Accordingly, the adjusted R^2 is computed for each index as follow:

$$adj.R^2 = 1 - \frac{df_t \times \tilde{r}_{yy}}{df_e} \tag{14}$$

where df_t is the degrees of freedom (N − 1) and df_e is the sum of squares for Error (N − p^c). N and p^c present effective sample size and the number of non-redundant parameters of the model, respectively. The calculated adjusted R^2 declaring how well the parameters fit the model is equal to 0.70, 0.76, and 0.85 for $CRBI_1$, $CRBI_2$, and $CRBI_3$, respectively. To detect the most important predictor of each index, a procedure based on the residual sum of squares (SSe) is carried out by removing one predictor at a time from the model. The predictor importance of X_i with p predictors is defined as:

$$I_i = \left(\tilde{r}_{yy}^{(i)} - \tilde{r}_{yy}\right)(N-1)SS_{yy} \tag{15}$$

where SS_{yy} is the weighted sample variance for y. The normalized I_i would be computed when p is less than i. The predictor importance of the developed indices is shown in Fig. 14 indicating the high relativity of the Melton ruggedness parameter in predicting the target values followed by the dam mean height in $CRBI_2$ and the dam volume in $CRBI_1$. The catchment mean slope displays the lowest importance by the maximum of 4 % involvement in $CRBI_2$.

4. Discussion

The presented database in this study includes both qualitative characteristics and geometric parameters of the detected landslide dams within a part of the Eastern Alps including Western Austria, Northern Italy, and Bavaria. The data is scattered in the forms of regional and time-dependent clusters. The regional distribution in specific valleys

(Inn, Ötz, Badia, etc.) indicates the role of the valley's characteristics in the resulted clusters. The shape of the valley is controlled by either fluvial (V-shape) or glacial (U-shape) processes though, the fluvial valleys are assumed to be twice narrower than glacial valleys at their downslope (Montgomery, 2002). As the result of fluvial modification of the post-glacial landscape, many of the V-shaped steep valleys show a firm tectonic control on river incision hence, the formation of the landslide dams is favored by the low accommodation space on the valley floors (Korup, 2005). The time-dependent distribution of the landslides generally points out the dependency of the failure events on either deglaciation, climatic fluctuations, or earthquakes. The evidence from dated landslide dams in this inventory supported the significance of some climatic fluctuations such as return to glacial condition (11.2 to 13.6 ka BP), cooling phase (8.2 ka BP), and increase of water supply and glacial advances in the Austrian Central Alps (3 to 4.2 ka BP) in the occurrence of the landslides. However, the fact that about 60 % of the landslides took place between 0 and 5000 BP, highlights the responsibility of the time-dependent rock slope weakening processes for the time lag of at least several thousand years between deglaciation and slope collapses. These rock slope weakening processes are an interplay between several factors: a) glacial loading and unloading (isostatic rebounds, stress redistribution, daylighting of sliding planes), b) fracture propagation clearly below critical rupture load (crack growth, progressive coalescence of discontinuities, material fatigue, increased fracture porosity), and c) disposition (petrography, fracture geometries, in-situ stresses, pore water characteristics, Subcritical crack growth/propagation, fracture density, persistence increase in time)(Prager et al., 2008). Therefore, the landslide eventually occurs when the rock mass strength threshold is exceeded.

The majority of landslide dammed-lakes in this inventory (71 % of the lakes) have disappeared through time. Nonetheless, a dam failure cannot be assigned to almost 40 % of these cases. Therefore, reservoir infill with sediments accounted for the processes that led to the disappearance of these backwater lakes. On one hand, this indicates the impact of damming process on the river morphology where, the sedimentation reflects the raised local base level to the lake height (Fan et al., 2020). On the other hand, it designates the influence of the contributing catchment by controlling the fluvial inlet into the lake. Based on previous observations, large landslides impound small lakes (Korup, 2004). This claim is supported by the outcomes of this study as the statistics of impoundments' volume show high kurtosis and skewness as well as the agreement of the minimum (1.6E−4 km^3) and median (1E−2 km^3) values in comparison to the maximum value (0.9 km^3). Furthermore, the extent of the upstream catchment in 62 % of the landslide dams is <100 km^2 which results in an inadequate discharge to form a large backwater lake.

To determine different evolution domains based on geomorphic indices, we considered a 95 % confidence interval of the mean value as the upper and lower bound, however, in the literature, the limits were set on absolute maximum and minimum values. The implemented statistical method led to a systematic approach affecting least by the exceptional geomorphic characteristics of the landslide dams. Nonetheless, we are forced to deal with some outlier cases. Overall 20 different cases have counted as outliers while examining the applicability of the thus far developed geomorphic indices on the presented data inventory. Among these cases, the Durchholzen (Tyrol, Austria) and Durnholzersee (South Tyrol, Italy) landslide dams repeated themselves frequently as outliers. The volume of the Durchholzen landslide dam as a formed-unstable case is estimated at about 80 Mm^3, however, the size of the watershed influencing the dam is only around 10 km^2. Regarding the small size of the watershed and large volume, this landslide dam lies in the stable domain. Though, the drainage of Walchsee lake 2 km upstream of the backwater sediments seems to be the reason for the fluvial incision in the landslide deposit and further instability (Fig. 15-a). On the other hand, the dam volume of the Durnholzersee as an existing lake is approximated 1.3 Mm^3 while the catchment area is
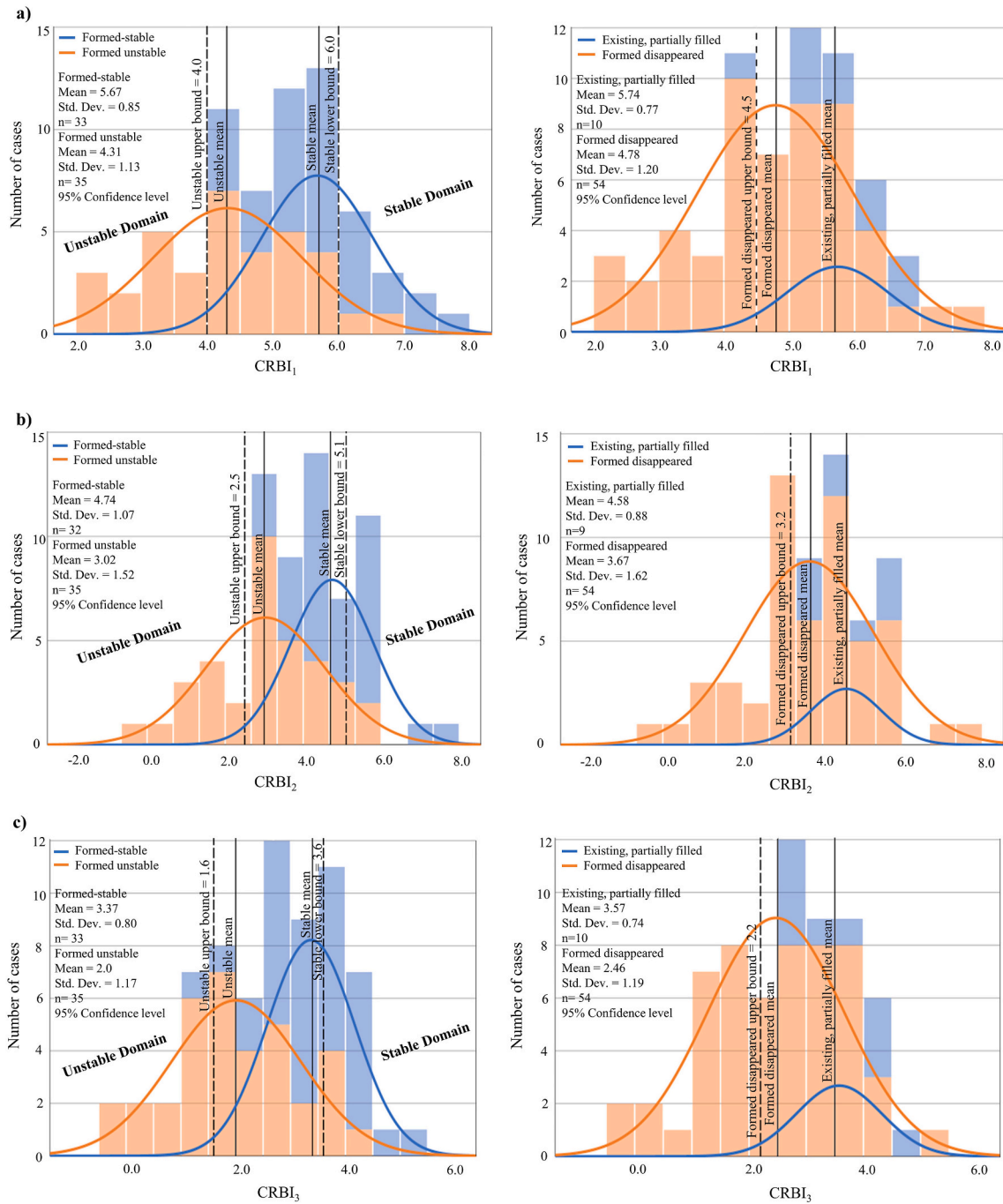
Fig. 12. Stacked histograms of the part of the Eastern Alps data inventory based on the developed geomorphic indices (a) $CRBI_1$ (b) $CRBI_2$ (c) $CRBI_3$ by dam evolution on the left and the lake evolution on the right side displaying the defined bounds considering 95 % confidence level of the mean value.

rather vast and encompasses 30 km². Due to the narrow width of the dammed valley (0.1 km) and the low spread of the deposited materials (area of the dam = 0.04 km²), the mean height of the dam is estimated at a rather high value of 35 m acting as the key parameter in keeping the dam stable (Fig. 15-b). Indeed, the Durnholzersee is only counted as an outlier when the indices don't include the effect of the dam height.

The performance of the so far developed geomorphic indices on the part of Eastern Alps data indicated the applicability of the catchment-based indices (blockage and dimensionless blockage) rather than indices depending on the volume of the lake as the destructive force (impoundment and backstow). The HDSI developed on the Italian database (Tacconi Stefanelli et al., 2016) displayed a high number of outliers (12 % of the whole data) when applied to the stable and unstable

landslide dams of the developed inventory, despite being based on the catchment area and the channel bed slope. The outliers for other indices mostly are observed above the stable lower limit where the contradiction could be justified by the catchment size. For this specific index, outliers have been detected at both stable and unstable domains. This shows the lack of efficiency of the resisting force (landslide volume) to accurately separate the data. In the presented database, the volume of the landslide for most of the cases is less than the corresponding dam. Then, due to the range of the landslide volume, there are some stable cases in the HDSI graph that fell below the unstable upper limit. A high number of outliers (between 7 % to 9 % of the whole data) is also observed for the indices relying on the height of the dam as the vertical separator (relief, basin, and backstow). The function of the height of the
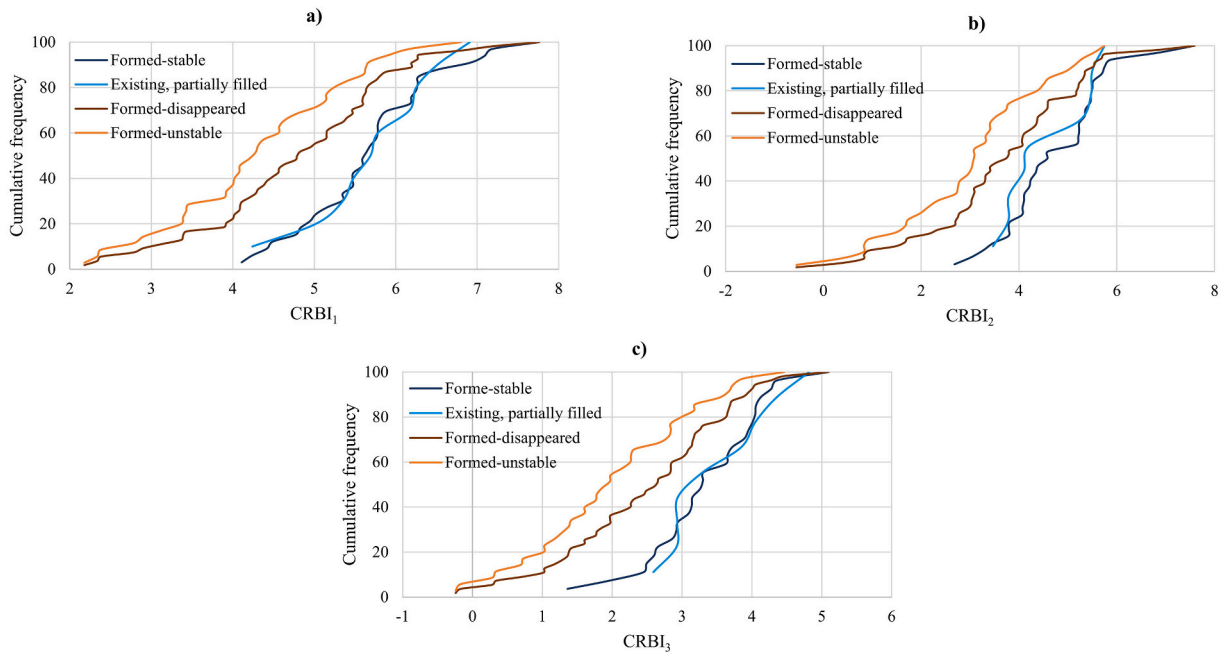
Fig. 13. Cumulative frequency of the part of the Eastern Alps data is shown based on the developed geomorphic indices (a) $CRBI_1$ (b) $CRBI_2$ (c) $CRBI_3$ separating the formed-stable from the formed-unstable dams at the left side and the existing, partially filled from the formed-disappeared lakes at the right side.
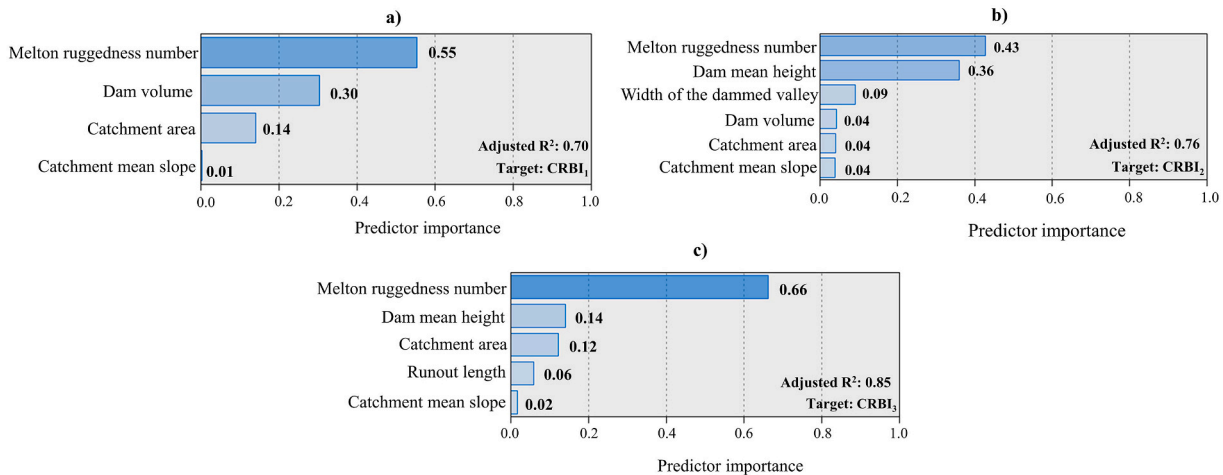
Fig. 14. Predictor importance of the developed geomorphic indices (a) $CRBI_1$ (b) $CRBI_2$ (c) $CRBI_3$ showing the high relativity of the Melton ruggedness number in predicting the targets (indices).

dam as a single indicator is also not efficient in defining domains for the presented database since the spread of the landslide deposit is neglected completely.

The catchment ruggedness-based indices developed in this study proceed upon the same driving force consisting of the catchment geometric properties. However, the importance of the catchment mean slope is estimated as <4 % in all the indices. We have omitted this parameter as it is preferred to have fewer variables in a developed formula. Without considering the mean slope of the catchment, the defined upper and lower bounds are getting closer causing a less wide uncertain domain for the $CRBI_1$ (66.1 % compared to 67.6 %). It reduces, on the other hand, the efficiency of two other indices by generating more outliers in $CRBI_2$ (4 outliers instead of 3) and increasing the percent of the data in the uncertain domain in $CRBI_3$ (60.3 % compared to 58.8 %). Due to the positive effect of the catchment mean slope on 2 out of 3 indices and the simple process of the parameter estimation, the formula has not been changed.

The reliability of the indices is confirmed by calculating the adjusted R^2 of >70 %, the existence of outliers <5 % of the data, and a quite narrower uncertain domain compared to the indices used in previous studies. Moreover, the applicability of the same driving force plotting with different parameters of the landslide and dam as resisting force shows the high efficiency of separation on the horizontal axis of the obtained diagrams. Overall 6 different landslide dams are detected as outliers in which Durchholzen repeated itself on all of the dam stability plots. The only outlier observed on the lake availability plots is Durnholzersee on $CRBI_1$. The narrowest stated uncertain domain in the literature belongs to the HDSI with 66 % of the data. Here, the $CRBI_2$ and $CRBI_3$ hold 61 % and 59 % of the data in the uncertain domain. However, the role of defining the boundaries based on the 95 % confidence level of the mean value should not be neglected.
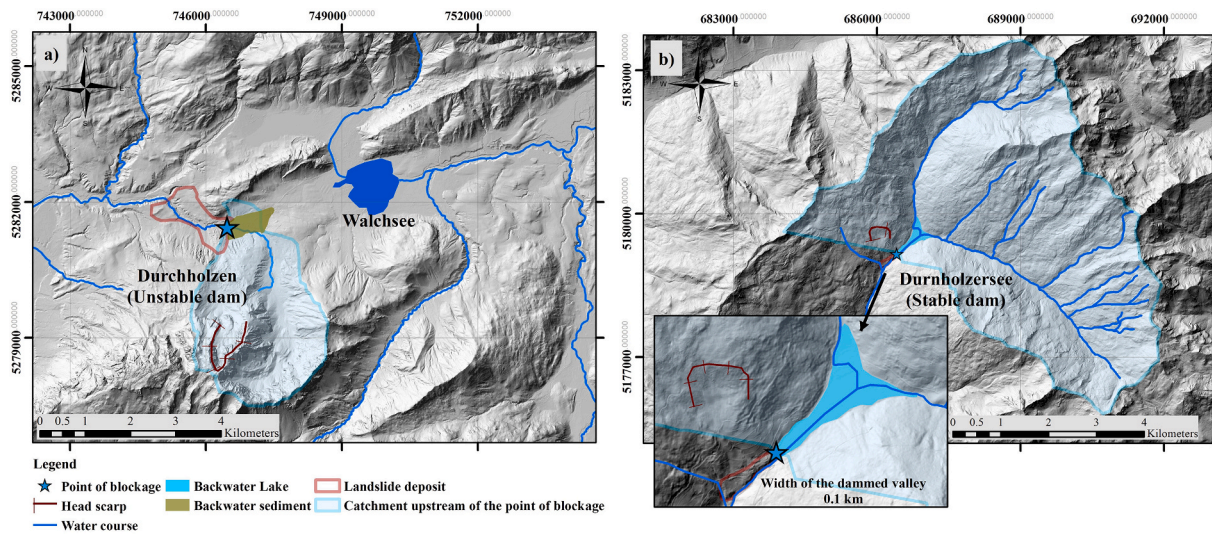
Fig. 15. Two of the most repeated outlier cases shown on the 5 m resolution DEMs (data.gv.at, geokatalog.bürgernetz.bz.it): a) The Durchholzen landslide dam is exposed to a rather small catchment (9.1 km^2) compare to the deposit volume (80 Mm^3), however, the dam went through the failure as the result of the Walchsee lake drainage. b) The Durnholzersee is under the influence of a relatively large catchment (30 km^2) but, due to the low runout length of the landslide, the height of the deposited material (35 m) increases the stability of the dam.

5. Summary and conclusions

A landslide dam database consisting of 73 cases is presented in this work. The measured and collected information about landslide dams is classified into the 5 categories of location, landslide, dam, lake, and catchment. The main findings during the data collection, parameter analyses and data interpretation are as follows:

- Estimation of the mean dam height based on the approximate range of the dam volume (10–30 % volume increase after the movement) caused a more precise estimation as the valley floor before the occurrence of the landslide is unknown most of the time. Considering the height of the dam in different cross-sections with constant spacing led to a moderate estimation of the height rather than assigning the maximum value to the whole area.
- Due to the high variability in the size of the landslide dam's backwater lakes, the upstream channel bed slope should be estimated based on the length of the formed lake (here, two times the length is considered). Applying a constant distance for different cases is not practical.
- Regarding the accessible information on occurrence date in the current database the majority of the cases belongs to Holocene age and about 60 % of them took place between 0 and 5000 BP. This indicates the role of climatic fluctuations and rock slope weakening processes in the slope collapses. Although, this claim can be improved by further detailed dating studies.
- Landslide dam evolution of the presented data indicated nearly the same amount of stable and unstable dams. The backwater lakes have disappeared in >70 % of the cases by either failure of the dam or sedimentation. The dam evolution in 28 % of the formed-disappeared lakes is considered stable which indicates the high rate of sedimentation in the Eastern Alps region.
- The unique geomorphic characteristics of the landslide dams caused a skewed distribution of the measured data which is detected by the difference between the median and mean values followed by the high kurtosis and skewness in the specific properties such as landslide volume, dam length, dam volume, and lake volume.
- Comparing the representative parameters of the landslide, dam, and lake with other data inventories, the Eastern Alps parameters are more compatible with the New Zealand database than with the Italian, despite the geographical location. This is due to the volume

difference between the largest landslide dams in the Italian (about 300 Mm^3) and the part of the Eastern Alps (about 3200 Mm^3) data inventories. The mean dam height of the part of the Eastern Alps, New Zealand, Japan, and the worldwide datasets varies between 51 and 67 m indicating a close estimation in different geographical regions.
- The geometric parameters of the dam specified a fairly strong correlation with some of the landslide and lake parameters, however, catchment and lake parameters are statistically independent of the landslide characteristics.

A good practice for the landslide dam inventories is to assess the stability of the dams by developing geomorphic indices based on a large set of data. At first, the applicability of the existing indices is assessed on the part of the Eastern Alps database by defining the index bounds on the 95 % confidence level of the mean value:

- Dimensionless blockage and blockage indices are applicable in separating the stable and unstable dams of the current database by not exceeding the outlier criterion (<5 % of the data) and including 60 and 65 % of the data in the uncertain domain.
- All the previously developed geomorphic indices are applicable in setting a bound on the formed-disappeared backwater lakes of the part of the Eastern Alps database. However, the best relevancy belongs to the dimensionless blockage index and impoundment index encompassing 37.5 % of the data within the established bound. Due to the few numbers of the existing, partially filled lakes, another bound is not defined in the lake availability plots.

To develop a reference on the landslide dams' stability for the Eastern Alps a set of catchment ruggedness-based indices (CRBI$_{1-3}$) is developed acting upon the same driving force (catchment area, catchment mean slope, and Melton ruggedness number) and three different sets of resisting forces based on parameters of the landslide and dam:

- By setting the resisting force as a combination of the dam mean height and landslide runout (CRBI$_3$), the narrowest uncertain zone (59 %) in the dam stability plot is obtained followed by the CRBI$_3$ (functioning based on the volume, mean height of the dam, and width of the dammed valley) showing 62 % of the data in the uncertain domain. The range of uncertain domains is improved

comparing the best-presented value in the literature (66 % of hydro-morphological dam stability index, Tacconi Stefanelli et al., 2016).

- The developed indices showed almost the same applicability in defining the upper bound of the formed-disappeared lakes by including 31–33 % of the data within the specified limits.
- According to the linear regression of the indices and the predictor parameters, the adjusted R^2 is the highest (0.85) for $CRBI_3$ follows by $CRBI_2$ (0.76), and $CRBI_1$ (0.70).
- Due to a predictor importance analysis on the indices (targets), the Melton ruggedness number is determined as the most important predictor (between 66 % and 43 %). The dam mean height and the dam volume also showed about 30 % importance in predicting $CRBI_1$ and $CRBI_2$ indices.

The data inventory and consequently, the developed indices are built upon the currently available literature and data hence, they can be updated following further research. An interesting practice to evaluate the applicability of the catchment ruggedness-based indices is to apply them to the other landslide dams' inventories around the world. This assessment is not carried out in this study due to the lack of information on some required parameters such as Melton ruggedness number, landslide runout length, and catchment mean slope in the published literature.

The stability of the landslide dams is predicted based on their estimated geometrical properties. Despite the constant and relatively accurate methods implemented in the estimation of these parameters, the geomorphic indices sometimes failed to anticipate the stability state of some of the cases in the data inventory. Therefore, the stability of a landslide dam, besides the geomorphological characteristics, relies also on other environmental and structural factors such as the hydraulic condition of the area and the geotechnical internal composition of the dam. Accordingly, facing the landslide dam hazard, a detailed study of the different engineering aspects of the landslide dam along with the geomorphological predictors is highly recommended.

Declaration of competing interest

The authors declare that they have no known competing financial interests or personal relationships that could have appeared to influence the work reported in this paper.

Acknowledgments

Appendix A

Table A.1
Description and main references of the information fields in the landslide dam database.

Category	Parameter	Description	Reference
Location	ID	Identification number for landslide	
	Name	The most common name referred to the landslide in literature, name of the location	Published papers, Google Earth
	Scarp midpoint, UTM, E N	The coordinate of the point in the middle of the landslide scarp, ETRS-1989-UTM-Zone-32N, 33N	
	Dam centroid, UTM, E N	The center coordinate of the dam, ETRS-1989-UTM-Zone-32N, 33N	
	UTM zone	UTM-Zone 32N or 33N	ArcGIS webpage
	Province/country	The geographic location of the landslide dam	Borders on Google earth
	Location in the Alps	Northern-Eastern, Central-Eastern or Southern-Eastern of Alps	Graßler's classification (1984)
	Mountain group	The mountain range in the Eastern Alps	Graßler's classification (1984)
	Related river	The name of the dammed, or deviated river	Open Data Austria (data.gv.at), Open street map
Landslide	Age	Date of landslide formation	Published papers
	Lithology/Era	Dominant lithology of the landslide area and the estimated era	Geological maps of Austria,1:500,000 (data.gv.at); South Tyrol, 1:25,000 (geokatalog.buergernetz.bz.it); Bavaria, 1:500,000 (ldbv.bayern.de); Europe, 1:5,000,000 (bgr.bund.de)
	Tectonic unit	Tectonic systems of the Alps	Schmid et al., 2004
	Height [H_L] (m)	The difference in elevation between the crown and the tip of the landslide	2.5–10 m-DEMs
	Runout angle [R_A] (°)	Material travel angle calculated based on the height of the landslide and the runout length	2.5–10 m-DEMs, published papers
	Runout length [R_L] (km)	The horizontal distance between the crown of the landslide and the farthest edge of the spread deposit	2.5–10 m-DEMs, published papers
	Volume [V_{rs}] (Mm^3)	The volume of the landslide before detachment	2.5–10 m-DEMs, published papers
Dam	Condition	The evolution of landslide dams under three classifications: formed stable, formed unstable, not formed	2.5–10 m-DEMs, satellite images, published papers
	Type	Geomorphic assessment of the landslide dams based on three-dimensional distribution of the landslide debris within the valley	Hermanns et al., 2011b
	Area [A_D] (km^2)	Area of the landslide deposit within the dammed valley	2.5–10 m-DEMs
	Length [L_D] (km)	The maximum length of the dam across the valley	2.5–10 m-DEMs
	Width [W_D] (km)	The maximum length of the dam along the valley	2.5–10 m-DEMs
	Mean height [H_D] (m)	The average maximum height between several cross-sections perpendicular to the dammed valley	2.5–10 m-DEMs, published papers
	Volume [V_D] (Mm^3)	The volume of the landslide deposit blocking the valley	2.5–10 m-DEMs, published papers
	Dam crest elevation [E_{min}] (m a.s.l.)	Maximum altitude of the dam	2.5–10 m-DEMs
	Width of the dammed valley [W_v] (km)	Maximum width of the dammed valley	2.5–10 m-DEMs

Table A.1 (*continued*)

Category	Parameter	Description	Reference
Lake	Condition	The current evolution of the backwater lake with three classifications: existing, partially filled; formed-disappeared; not formed	2.5–10 m-DEMs, satellite images, published papers
	Area [A_L] (km^2)	The area of the backwater lake	2.5–10 m-DEMs
	Length [L_L] (km)	The maximum length of the lake along the river axis	2.5–10 m-DEMs
	Width [W_L] (km)	The maximum length of the lake across the river axis	2.5–10 m-DEMs
	Mean depth [D_L] (m)	The average depth of the lake	2.5–10 m-DEMs
	Volume [V_L] (Mm^3)	Approximate volume of the natural impoundment	2.5–10 m-DEMs
	Mean channel bed slope [S] (m/m)	The gradient between doubled lake length upstream and lake length downstream of the point of blockage	2.5–10 m-DEMs
	Upstream channel bed slope (m/m)	The gradient of doubled lake length upstream of the point of blockage	2.5-10 m-DEMs
	Downstream channel bed slope (m/m)	The gradient of the lake length downstream of the point of blockage	2.5-10 m-DEMs
Catchment	Area [A_C] (km^2)	Catchment area upstream of the point of blockage	2.5-10 m-DEMs
	Maximum altitude [E_{max}] (m a.s.l.)	Maximum altitude in the catchment area upstream of the point of blockage	2.5-10 m-DEMs
	Relief [H_R] (m)	Relief upstream of the point of blockage [$H_R = E_{max}-(E_{min}-H_D)$]	2.5-10 m-DEMs
	Relief ratio [R_r] (m/km^2)	The ratio of relief versus the catchment area	2.5-10 m-DEMs
	Mean slope [C_s] (°)	Mean terrain slope of the catchment	2.5-10 m-DEMs
	Melton ruggedness number [MRN]	Difference between maximum and minimum elevation in the catchment area divided by the square root of the catchment area size	2.5-10 m-DEMs

Appendix B

Table B.1
Summary of the defined bounds of the previously developed geomorphic indices.

Index	Domain	Index bound	Data within the uncertain domain (%)	Reference
Blockage (BI)	Existing lake	BI > 7	–	Korup (2004)
	Formed-disappeared lake	2 < BI < 4		
	Not formed lake	BI < 2		
	Formed dam	BI > 5.68	81	Tacconi Stefanelli et al. (2016)
	Not formed dam	BI < 3.00		
Impoundment (I_i)	Existing lake	Ii > 1.0	–	Korup (2004)
Dimensionless blockage (DBI)	Stable dam	DBI < 2.75	–	Ermini and Casagli (2003)
	Unstable dam	DBI > 3.00		
	Existing lake	DBI > 5	–	Korup (2004)
	Formed-disappeared lake	DBI < 3		
	Stable dam	DBI < 2.43	76	Tacconi Stefanelli et al. (2016)
	Unstable dam	DBI > 3.98		
Backstow (I_a)	Stable dam	I_s < −3	–	Korup (2004)
	Unstable dam	I_s > 0		
Basin (I_a)	Existing lake	I_a > 3	–	Korup (2004)
Relief (I_r)	Existing lake	I_r > −1	–	Korup (2004)
Hydromorphological dam stability (HDSI)	Stable dam	HDSI > 7.44	66	Tacconi Stefanelli et al. (2016)
	Unstable dam	HDSI < 5.74		
	Stable dam	HDSI > 8.07	72	Tacconi Stefanelli et al. (2018)
	Unstable dam	HDSI < 5.26		
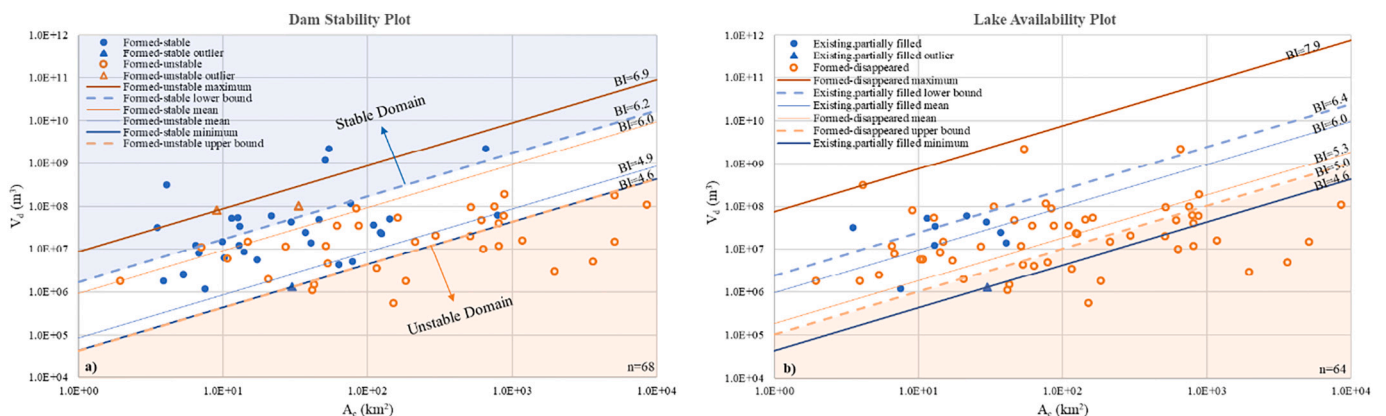
Fig. B.1. (a) Dam stability and (b) lake availability plots of the part of the Eastern Alps inventory based on the blockage index.
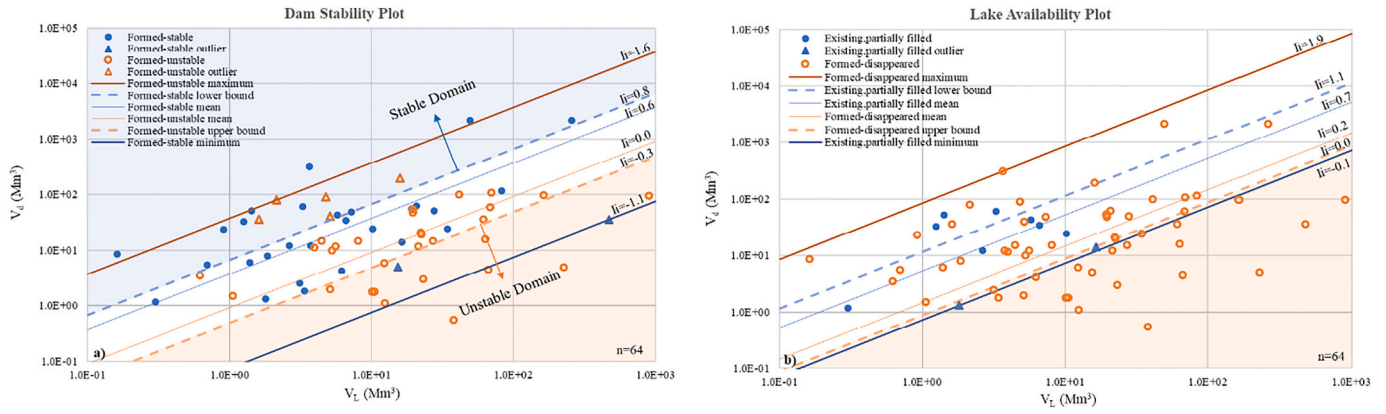
Fig. B.2. (a) Dam stability and (b) lake availability plots of the part of the Eastern Alps inventory based on the impoundment index.
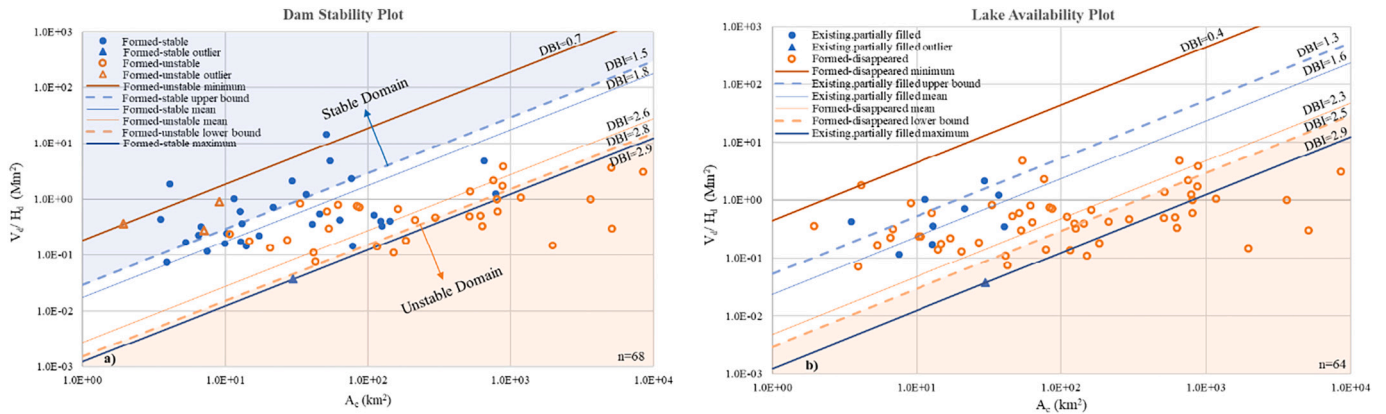
Fig. B.3. (a) Dam stability and (b) lake availability plots of the part of the Eastern Alps inventory based on the dimensionless blockage index.
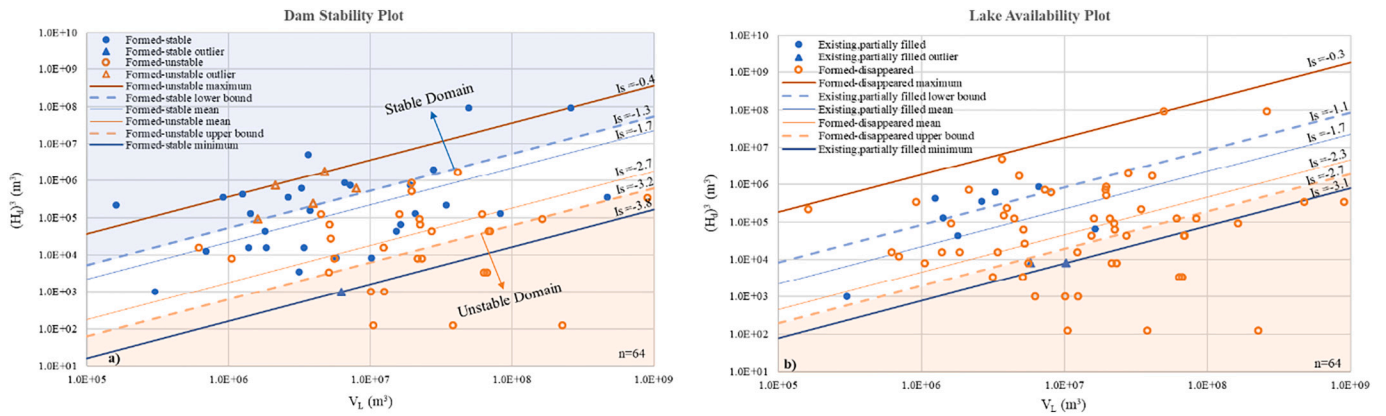
Fig. B.4. (a) Dam stability and (b) lake availability plots of the part of the Eastern Alps inventory based on the backstow index.
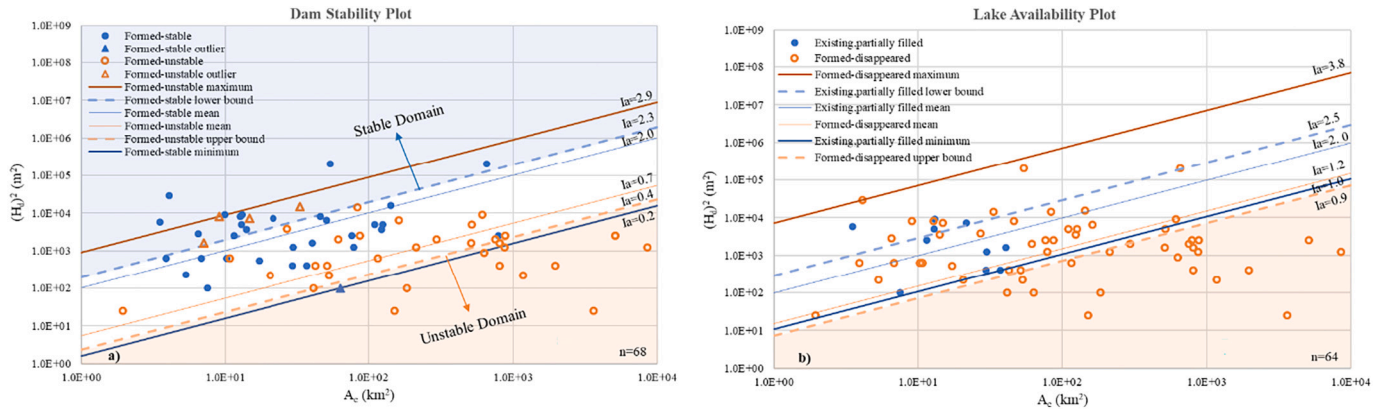
Fig. B.5. (a) Dam stability and (b) lake availability plots of the part of the Eastern Alps inventory based on the basin index.
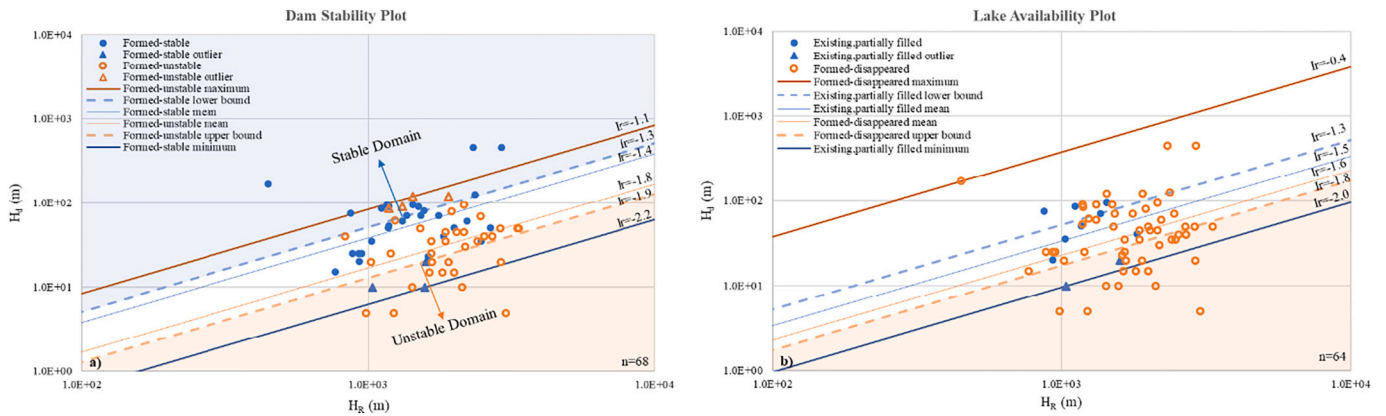
Fig. B.6. (a) Dam stability and (b) lake availability plots of the part of the Eastern Alps inventory based on the relief index.
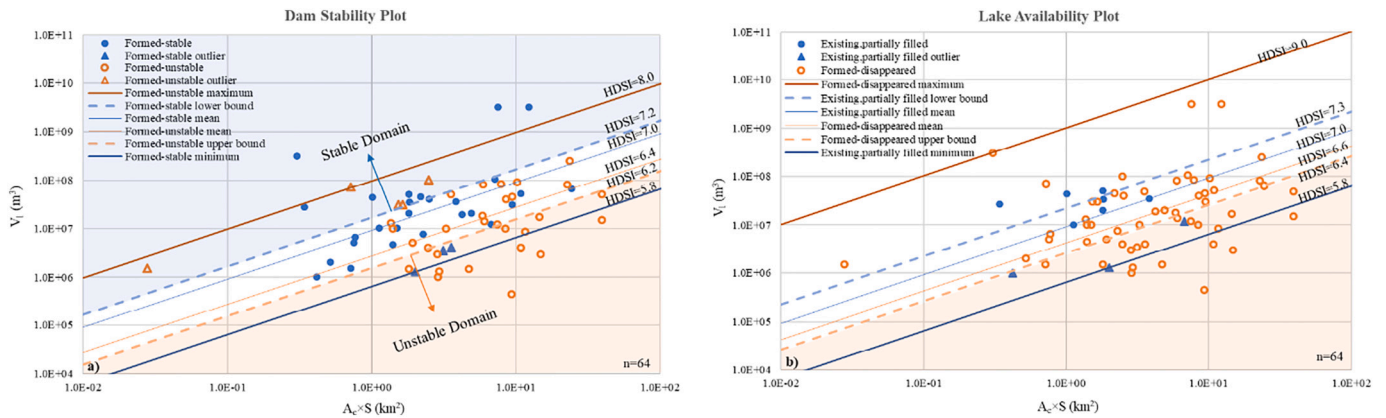
Fig. B.7. (a) Dam stability and (b) lake availability plots of the part of the Eastern Alps inventory based on the hydro-morphological dam stability index.

Appendix C. Supplementary data

The supplementary data comprising of:

- A GIs Geodatabase including relevant shapefiles of the database.
- The measured and calculated parameters of the landslide dams as excel file.
- The table of measured and calculated parameters of the landslide dams as pdf file.

Supplementary data to this article can be found online at https://doi.org/10.1016/j.geomorph.2022.108403.

References

Abele, G., 1974. Bergstürze in den Alpen, ihre Verbreitung, Morphologie und Folgeerscheinungen. Wiss. Alpenvereinshefte 25 (230 pp.).

Bertoni, G., 1843. Memoria sul Lago di Quarto nella legazione di Forlì. Tipografia delle Belle Arti, tav. Roma 28, 1.

Bonnard, C., 2011. Technical and human aspects of historic rockslide-dammed lakes and landslide dam breaches. In: Evans, S., Hermanns, R., Strom, A., Scarascia-Mugnozza, G. (Eds.), Natural and Artificial Rockslide Dams, Lecture Notes in Earth Sci, vol. 133. Springer, Berlin, Heidelberg, pp. 101–122. https://doi.org/10.1007/978-3-642-04764-0_3.

Bunn, M., Leshchinsky, B., Olsen, M., 2020. Estimates of three-dimensional rupture surface geometry of deep-seated landslides using landslide inventories and high-resolution topographic data. Geomorphology 367, 107332. https://doi.org/10.1016/j.geomorph.2020.107332.

Canuti, P., Casagli, N., Ermini, L., 1998. Inventory of landslide dams in the Northern Apennine as a model for induced flood hazard forecasting. In: Andah, K. (Ed.), Managing hydro-geological disasters in a vulnerable environment for sustainable development, 1900. CNR-GNDCI-UNESCO (IHP), Perugia, pp. 189–202.

Casagli, N., Ermini, L., 1999. Geomorphic analysis of landslide dams in the Northern Apennine. Trans. Jpn. Geomorphol. 20 (3), 219–249 (ISSN: 03891755).

Costa, J.E., Schuster, R.L., 1988. The formation and failure of natural dams. Geol. Soc. Am. Bull. 100 (7), 1054–1068. https://doi.org/10.1130/0016-7606(1988)100<1054:TFAFON>2.3.CO;2.

Costa, J.E., Schuster, R.L., 1991. Documented historical landslide dams from around the world. In: USGS Open-File Report, 91-239. https://doi.org/10.3133/ofr91239.

Cotza, G., 2009. Geologische und geotechnische Verhältnisse der Massenbewegungen bei Pontives (Grödnertal, Südtirol). University of Vienna. https://doi.org/10.25365/thesis.6143 (Master Thesis).

Curden, D.M., Varnes, D.J., 1996. Landslide types and processe. In: Schuster, R.L., Turner, A.K. (Eds.), Landslides: Investigation and mitigation. Transp. Research Board, Washington: NAP, pp. 36–75.

Dai, F.C., Lee, C.F., Deng, J.H., Tham, L.G., 2005. The 1786 earthquake-triggered landslide dam and subsequent dam-break flood on the Dadu River, southwestern China. Geomorphology 65 (3–4), 205–221. https://doi.org/10.1016/j.geomorph.2004.08.011.

Delaney, K.B., Evans, S.G., 2015. The 2000 Yigong landslide (Tibetan Plateau), rockslide-dammed lake and outburst flood: Review, remote sensing analysis, and process modelling. Geomorphology 246, 377–393. https://doi.org/10.1016/j.geomorph.2015.06.020.

Domej, G., Bourdeau, C., Lenti, L., Martino, S., Pluta, K., 2020. Shape and dimension estimation of landslide rupture zones via correlations of characteristic parameters. Geosci. 10 (5), 198. https://doi.org/10.3390/geosciences10050198.

Dong, J.J., Tung, Y.H., Chen, C.C., Liao, J.J., Pan, Y.W., 2009. Discriminant analysis of the geomorphic characteristics and stability of landslide dams. Geomorphology 110 (3–4), 162–171. https://doi.org/10.1016/j.geomorph.2009.04.004.

Dufresne, A., Prager, C., Bösmeier, A., 2016. Insights into rock avalanche emplacement processes from detailed morpho-lithological studies of the Tschirgant deposit (Tyrol, Austria). Earth Surf. Process. Landf. 41 (5), 587–602. https://doi.org/10.1002/esp.3847.

Dufresne, A., Ostermann, M., Preusser, F., 2018. River-damming, late-Quaternary rockslides in the Ötz Valley region (Tyrol, Austria). Geomorphology 310, 153–167. https://doi.org/10.1016/j.geomorph.2018.03.012.

Eisbacher, G., Clague, J.J., 1984. Destructive mass movements in high mountain: hazard and management. Geol. Surv. Can. Paper 84-16. https://doi.org/10.2307/1550874.

Ermini, L., Casagli, N., 2003. Prediction of the behaviour of landslide dams using a geomorphological dimensionless index. Earth Surf. Process. Landf. 28 (1), 31–47. https://doi.org/10.1002/esp.424.

Fan, X., van Westen, C.J., Korup, O., Gorum, T., Xu, Q., Dai, F., Huang, R., Wang, G., 2012. Transient water and sediment storage of the decaying landslide dams induced by the 2008 Wenchuan earthquake, China. Geomorphology 171-172, 58–68. https://doi.org/10.1016/j.geomorph.2012.05.003.

Fan, X., Dufresne, A., Subramanian, S.S., Strom, A., Hermanns, R., Tacconi Stefanelli, C., Hewitt, K., Yunus, A.P., Dunning, S., Capra, L., Geertsema, M., Miller, B., Casagli, N., Jansen, J.D., Xu, Q., 2020. The formation and impact of landslide dams – state of the art. Earth Sci. Rev. 203, 103–116. https://doi.org/10.1016/j.earscirev.2020.103116.

Felber, H., 1987. Vienna radium institute radiocarbon dates XVI. Radiocarbon 29 (3), 389–396.

Ferrer, C., 1999. Represamientos y rupturas de embalses naturales (lagunas de obstrución) como efectos cosísmicos: Algunos ejemplos en los Andes venezolanos. Rev. Geogr. Venez. 40 (1), 109–121 (ISSN: 10121617).

Graßler, F., 1984. Alpenvereinseinteilung der Ostalpen (AVE). In: DAV, ÖAV, AVS (Eds.), Berg 84, Folguera, A., Penna, I., Fauqué, L., Niedermann, S., 2011a. Landslide 1984.

Gruber, A., Strauhal, T., Prager, C., Reitner, J.M., Brandner, R., Zangerl, C., 2009. Die «Butterbichl-Gleitmasse» - eine große fossile Massenbewegung am Südrand der Nördlichen Kalkalpen (Tirol, Österreich). Swiss Bull. Angew. Geol. 14 (1–2), 103–134.

Hermanns, R.L., 2013. Landslide dam. In: Bobrowsky, P.T. (Ed.), Encyclopedia of natural hazards. Encycl. Earth Sci. Series, Dordrecht, pp. 602–606. https://doi.org/10.1007/978-1-4020-4399-4_213.

Hermanns, R.L., Folguera, A., Penna, I., Fauqué, L., Niedermann, S., 2011a. Landslide dams in the Central Andes of Argentina (Northern Patagonia and the Argentine Northwest). In: Evans, S., Hermanns, R., Strom, A., Scarascia-Mugnozza, G. (Eds.), Natural and Artificial Rockslide Dams, Lecture Notes in Earth Sci., vol. 133.

Springer, Berlin, Heidelberg, pp. 147–176. https://doi.org/10.1007/978-3-642-04764-0_5.

Hermanns, R.L., Hewitt, K., Strom, A.L., Evans, E.G., Dunning, S.A., Scarascia-Mugnozza, G., 2011b. The classification of rock slide dams. In: Evans, S.G., Hermanns, R.L., Strom, A., Scarascia Mugnozza, G. (Eds.), Natural and Artificial Rockslide Dams, Lecture Series in Earth Sci.. Springer, Berlin, Heidelberg, pp. 581–593. https://doi.org/10.1007/978-3-642-04764-0.

Hewitt, K., 2011. Rock avalanche dams on the Trans Himalayan upper Indus streams: a survey of late Quaternary events and hazard-related characteristics. In: Evans, S., Hermanns, R., Strom, A., Scarascia-Mugnozza, G. (Eds.), Natural and Artificial Rockslide Dams, Lecture Notes in Earth Sci., vol. 133. Springer, Berlin, Heidelberg, pp. 177–204. https://doi.org/10.1007/978-3-642-04764-0_6.

Hutchinson, J.N., 1983. Methods of locating slip surfaces in landslides. Bull. Int. Assoc. Eng. Geol. 20 (3), 235–252. https://doi.org/10.2113/gseegeosci.xx.3.235.

Ivy-Ochs, S., Heuberger, H., Kubik, P.W., Kerschner, H., Bonani, G., Frank, M., Schluchter, C., 1998. The age of the Köfels event. Relative, 14C and cosmogenic isotope dating of an early Holocene landslide in the Central Alps (Tyrol, Austria). Zs. Gletscherkd. Glazialgeol. 34, 57–68 (Corpus ID: 128099251).

Jerz, H., 1999. Nacheiszeitliche Bergstürze in den Bayerischen Alpen. Relief Boden Klima 14, 31–40.

Knapp, S., Mamot, P., Lempe, B., Krautblatter, M., 2020. Impact of an 0.2 km^3 rock avalanche on Lake Eibsee (Bavarian Alps, Germany) – part I: reconstruction of the paleolake and effects of the impact. Earth Surf. Process. Landf. 46 (1), 296–306. https://doi.org/10.1002/esp.5024.

Korup, O., 2004. Geomorphic characteristics of New Zealand landslide dams. Eng. Geol. 73 (1–2), 13–35. https://doi.org/10.1016/j.enggeo.2003.11.003.

Korup, O., 2005. Geomorphic hazard assessment of landslide dams in South Westland, New Zealand: fundamental problems and approaches. Geomorphology 66, 167–188. https://doi.org/10.1016/j.geomorph.2004.09.013.

Korup, O., 2011. Rockslide and rock avalanche dams in the Southern Alps, New Zealand. In: Evans, S., Hermanns, R., Strom, A., Scarascia-Mugnozza, G. (Eds.), Natural and Artificial Rockslide Dams, Lecture Notes in Earth Sci., vol. 133. Springer, Berlin, Heidelberg, pp. 123–145. https://doi.org/10.1007/978-3-642-04764-0_4.

Korup, O., Wang, G., 2015. Chapter 8-multiple landslide-damming episodes. In: Shroder, J.F., Davies, T. (Eds.), Landslide Hazards, Risks and Disasters, Hazards and Disasters Series. Academic Press, pp. 241–261. https://doi.org/10.1016/B978-0-12-396452-6.00008-2.

Marchi, L., Dalla Fontana, G., 2005. GIS morphometric indicators for the analysis of sediment dynamics in mountain basins. Environ. Geol. 48, 218–228. https://doi.org/10.1007/s00254-005-1292-4.

Melton, M.A., 1965. The geomorphic and paleoclimatic significance of alluvial deposits in southern Arizona. J. Geol. 73 (1), 1–38.

Montgomery, D.R., 2002. Valley formation by fluvial and glacial erosion. Geol. 30 (11), 1047–1050. https://doi.org/10.1130/0091-7613(2002)030<1047:VFBFAG>2.0.CO;2.

Morche, D., Katterfeld, C., Fuchs, S., Schmidt, K.H., 2006. The life-span of a small high mountain lake, the Vordere Blaue Gumpe in Upper Bavaria, Germany. In: Rowan, J., Duck, R.W., Werritty, A. (Eds.), Sediment Dynamics and the Hydromorphology of Fluvial Systems. IAHS Press, Wallingford, UK, ISBN 1901502686, pp. 72–81.

Ostermann, M., Prager, C., 2016. Field trip 12, Rock slope failures shaping the landscape in the Loisach-, Inn- and Ötz Valley region (Tyrol, Austria). Geo.Alp 13, 257–276.

Ostermann, M., Sanders, D., 2017. The Benner pass rock avalanche cluster suggests a close relation between long-term slope deformation (DSGSDs and translational rock slides) and catastrophic failure. Geomorphology 289, 44–59. https://doi.org/10.1016/j.geomorph.2016.12.018.

Ostermann, M., Sanders, D., Prager, C., Kramers, J., 2007. Aragonite and calcite cementation in "boulder-controlled" meteoric environments on the Fern Pass rockslide (Austria): implications for radiometric age dating of catastrophic mass movements. Facies 53 (2), 189–208. https://doi.org/10.1007/s10347-006-0098-5.

Ostermann, M., Sanders, D., Ivy-Ochs, S., Alfimov, V., Rockenschaub, M., Römer, A., 2012. Early Holocene (8.6 ka) rock avalanche deposits, Obernberg valley (Eastern Alps): landform interpretation and kinematics of rapid mass movement. Geomorphology 171-172, 83–93. https://doi.org/10.1016/j.geomorph.2012.05.006.

Ostermann, M., Ivy-Ochs, S., Sanders, D., Prager, C., 2017. Multi-method (14C, 36Cl, 234U/230Th) age bracketing of the Tschirgant rock avalanche (Eastern Alps): implications for absolute dating of catastrophic mass-wasting. Earth Surf. Process. Landf. 42 (7), 1110–1118. https://doi.org/10.1002/esp.4077.

Ostermann, M., Ivy-Ochs, S., Ruegenberg, F., Vockenhuber, C., 2020. Characteristics and dating of the rock avalanche at Pragser Wildsee/Lago di Braies (Dolomites, Italy). Alp. Mediterr. Quat. 33 (2), 183–189. https://doi.org/10.26382/AMQ.2020.07.

Panizza, M., Corsini, A., Ghino, A., Marchetti, M., Pasuto, A., Soldati, M., 2011. Explanatory notes of the geomorphological map of the Alta Badia valley (Dolomites, Italy). Geogr. Fis. Din. Quat. 34, 105–126 (ISSN: 03919838).

Patton, P.C., 1988. Drainage basin morphometry and floods. In: Baker, V.R., Kochel, R.C., Patton, P.C. (Eds.), Flood Geomorphology. Wiley, New York, pp. 51–65. https://doi.org/10.1002/esp.3290150314.

Patzelt, G., 2012. Die Bergstürze vom Pletzachkogel, Kramsach. Tirol. Jb. Geol. B.-A. 152, 25–38 (ISSN 0016-7800).

Pearson, K., 1948. Early Statistical Papers. Univ. Press, Cambridge, England, pp. 339–357.

Peng, M., Zhang, L.M., 2012. Breaching parameters of landslide dams. Landslides 9, 13–31. https://doi.org/10.1007/s10346-011-0271-y.

Pirocchi, A., 1992. Laghi di sbarramento per frana nelle Alpi: tipologia ed evoluzione. In: Proceedings I Convegno Nazionale dei Giovani Ricercatori in Geologia Applicata,

GargnanoRicerca Scientifica Ed Educazione Permanente Vol. Suppl. 93. University of Milan, Milan, pp. 128–136.

Poschinger, A., Thom, P., 1995. Bergsturz Hintersee/Ramsau (Berchtesgadener Land): Neue Untersuchungsergebnisse. Geol. Bavarica 99, 399–411.

Prager, C., Krainer, K., Seidl, V., Chwatal, W., 2006. Spatial features of Holecen Sturzstorm-Deposits inferred from subsurface investigations (Fernpaß rockslide, Tyrol, Austria). Geol. Alps 3, 147–166 (Corpus ID: 9340214).

Prager, C., Zangerl, C., Patzelt, G., Brandner, R., 2008. Age distribution of fossil landslides in the Tyrol (Austria) and its surrounding areas. Nat. Hazards Earth Syst. Sci. 8 (2), 377–407. https://doi.org/10.5194/nhess-8-377-2008.

Prager, C., Ivy-Ochs, S., Ostermann, M., Synal, H.A., Patzelt, G., 2009a. Geology and radiometric 14C-, 36Cl- and Th-/U-dating of the Fernpass rockslide (Tyrol, Austria). Geomorphology 103 (1), 93–103. https://doi.org/10.1016/j.geomorph.2007.10.018.

Prager, C., Zangerl, C., Nagler, T., 2009b. Geological controls on slope deformations in the Köfels rockslide area (Tyrol, Austria). Austrian J. Earth Sci. 102 (2), 4–19.

Reitner, J.M., Ivy-Ochs, S., Hajdas, I., Lattner, D., 2014. Bergstürze in den Lienzer Dolomiten vom WürmSpätglazial bis in das jüngste Holozän. In: Koinig, K.A., Starnberger, R., Spötl, C. (Eds.), DEUQUA 2014: 37 Hauptversammlung der deutschen Quartärvereinigung Innsbruck, 37, September, Abstractband. Innsbruck Univ. Press, Innsbruck, pp. 24–29.

Reitner, J.M., Ivy-Ochs, S., Steinemann, O., Lattner, D., Römer, A., 2020. The early Holocene Buchwiese rock avalanche (Eastern Alps, Austria): geological conditions, kinematics, morphological and sedimentary legacy. Alp. Mediterr. Quat. 33 (2), 165–181. https://doi.org/10.26382/AMQ.2020.12.

Reuther, A.U., Reitner, J.M., Ivy-Ochs, S.W., Herbst, P., 2006. From kinematics to dating the Sturzstrom deposit of Feld (Matrei/Eastern Tyrol/Austria). Geophys. Res. Abstr. 8, 04947.

Schmid, S.M., Fügenschuh, B., Kissling, E., Schuster, R.L., 2004. Tectonic map and overall architecture of the Alpine orogen. Eclogae Geol. Helv. 97, 93–117. https://doi.org/10.1007/s00015-004-1113-x.

Schrott, L., Hufschmidt, G., Hankammer, M., Hoffmann, T., Dikau, R., 2003. Spatial distribution of sediment storage types and quantification of valley fill deposits in an alpine basin, Reintal, Bavarian Alps, Germany. Geomorphology 55 (1–4), 45–63. https://doi.org/10.1016/S0169-555X(03)00131-4.

Schuster, R.L., Alford, D., 2004. Usoi Landslide Dam and Lake Sarez, Pamir Mountains, Tajikistan. Environ. Eng. Geosci. 10 (2), 151–168. https://doi.org/10.2113/10.2.151.

Starnberger, R., Drescher-Schneider, R., Reitner, J.M., Rodnight, H., Reimer, P.J., Spötl, C., 2013. Late Pleistocene climate change and landscape dynamics in the Eastern Alps: the inner-alpine Unterangerberg record (Austria). Quat. Sci. Rev. 68, 17–42. https://doi.org/10.1016/j.quascirev.2013.02.008.

Stefani, M., Mantovani, M., Mair, V., Marcato, G., Pasuto, A., Nössing, L., 2013. The Ganderberg landslide (South Tyrol, Italy): mitigation of residual risk by real-time monitoring. In: Margottini, C., Canuti, P., Sassa, K. (Eds.), Early Warning, Instrumentation and Monitoring, Landslide Sci. and Practice, vol. 2. Springer-Verlag, Berlin Heidelberg, pp. 531–535.

Strom, A., Abdrakhmatov, K., 2018. Rockslides and Rock Avalanches of Central Asia: Distribution, Morphology, and Internal Structure. Elsevier, ISBN 978-0-12-803204-6 (443 p.).

Stuiver, M., Reimer, P.J., 1993. Extended 14C database and revised CALIB radiocarbon calibration program. Radiocarbon 35, 215–230. https://doi.org/10.1017/S0033822200013904.

Swanson, F.J., Oyagi, N., Tominaga, M., 1986. Landslide dams in Japan. In: Schuster, R. L. (Ed.), Landslide Dams: Processes risk and mitigation, , Geotechnical Special Publication3. Am. Soc. Civ. Eng., New York, pp. 131–145.

Tacconi Stefanelli, C., Catani, F., Casagli, N., 2015. Geomorphological investigations on landslide dams. Geoenviron. Disasters 2 (21), 1–15. https://doi.org/10.1186/s40677-015-0030-9.

Tacconi Stefanelli, C., Segoni, S., Casagli, N., Catani, F., 2016. Geomorphic indexing of landslide dams evolution. Eng. Geol. 208, 1–10. https://doi.org/10.1016/j.enggeo.2016.04.024.

Tacconi Stefanelli, C., Vilimek, V., Emmer, A., Catani, F., 2018. Morphological analysis and features of the landslide dams in the Cordillera Blanca, Peru. Landslides 15, 507–521. https://doi.org/10.1007/s10346-017-0888-6.

Uhlir, C.F., Schramm, J.M., 2003. Zur Kinematik des Bergsturzes von Vigaun (Salzburg). Mitt. Österr. Geol. Ges. 93, 161–173 (ISSN 0251-7493).

Wang, G., Furuya, G., Zhang, F., Doi, I., Watanabe, N., Wakai, A., Marui, H., 2016. Layered internal structure and breaching risk assessment of the Higashi-Takezawal landslide dam in Niigata, Japan. Geomorphology 267, 48–58. https://doi.org/10.1016/j.geomorph.2016.05.021.

Zangerl, C., Schneeberger, A., Steiner, G., Mergili, M., 2020. Geographic-information-system-based topographic reconstruction and geomechanical modelling of the Köfels Rock Slide. Nat. Hazards Earth Syst. Sci. 21 (8), 2461–2483. https://doi.org/10.5194/nhess-21-2461-2021.

Web references

DGM 2.5 m, South Tyrol. http://geokatalog.buergernetz.bz.it/geokatalog/#!home, 2006–. (Accessed February 2021).

DGM 5 m, airborne laser scan data (EPSG: 31258), Carinthia. https://www.data.gv.at/katalog/dataset/a188992b-4071-45c3-99ce-65662395ebe6. (Accessed February 2021).

DGM 5 m, airborne laser scan data (EPSG: 31258), Salzburg, 2007–2016. https://www.data.gv.at/katalog/dataset/digitales-gelandemodell-des-landes-salzburg-5m. (Accessed February 2021).

DGM 5 m, airborne laser scan data (EPSG: 31254), Tyrol. https://www.data.gv.at/katalog/dataset/land-tirol_tirolgelnde. (Accessed February 2021).

DGM 5 m, Bavaria. https://www.ldbv.bayern.de/produkte/3dprodukte/gelaende.html. (Accessed March 2021).

DGM 10 m, airborne laser scan data (EPSG: 31287). http://www.geoland.at. (Accessed October 2020).

Geological map, 1:50,000, Austria. https://gisgba.geologie.ac.at/arcgis/rest/services/image/AT_GBA_GEOFAST/ImageServer. (Accessed February 2022).

Geological map, 1:500,000, Bavaria. https://www.lfu.bayern.de/geologie/geo_karten_schriften/gk500/index.htm. (Accessed March 2021).

Geological map, 1:25,000, South Tyrol. http://geokatalog.buergernetz.bz.it/geokatalog/#!home. (Accessed March 2021).

IBM, 2015. IBM SPSS Modeler 17 Algorithms Guide, pp. 271–283. ftp://public.dhe.ibm.com/software/analytics/spss/documentation/modeler/17.0/en/AlgorithmsGuide.pdf. (Accessed December 2021).

International geological map of Europe and adjacent areas (IGME 5000), 1:5,000,000. https://www.bgr.bund.de/DE/Themen/Sammlungen-Grundlagen/GG_geol_Info/Karten/Europa/IGME5000/igme5000_inhalt.html. (Accessed April 2021).